Report:

EU FP6 Project UpWind

Integrated Wind Turbine Design (WP3.2)

Deliverable D.3.2.1b

Stiffness Degradation Models

Janis Varna

Dept of Applied Physics and Mechanical Engineering
Luleå University of Technology
Sweden

Contents

ABSTRACT:

A theoretical framework which allows determining the whole set of 2-D thermo-mechanical constants of a damaged laminate as a function of intralaminar crack density in different layers is presented. In this approach closed form expressions, which contain thermo-elastic ply properties, laminate lay-up and intralaminar crack density as the input information are obtained. It is shown that the crack face opening displacement (COD) and crack face sliding displacement, normalized with respect to a load variable, are important parameters in these expressions influencing the level of the properties degradation. They are determined using generalized plain strain FEM analysis results for non-interactive cracks. The strong dependence of the COD on the relative stiffness and thickness of the surrounding layers, found in this study, is described by a power law. The methodology is validated and the possible error introduced by the non-interactive crack assumption is estimated by comparing with the 3-D FEM solution for a cross-ply laminate with two orthogonal systems of ply-cracks. Experimental data and comparison with other models are used for further verification.

Stiffness of a unidirectional composite (UD) containing fiber breaks with partial debonding is analyzed. Using divergence theorem exact relationships are obtained which link the entire stiffness matrix of the damaged UD composite with two robust parameters from the local solution: average opening displacement (COD) of the fiber break and its sliding displacement (CSD). Both are normalized with respect to the size of the fiber crack and to the far field stress in the fiber. The effect of the partial fibe/matrix debonding at the interface is included in the model through increasing crack opening.

Using parametric inspection of obtained expressions it was shown that CSD does not affect the longitudinal stiffness and the COD effect on transverse and shear modulus and Poisson's ratio of the damaged composite is negligible. It motivated the decision to focus on COD and the longitudinal modulus. In this paper cracks are considered as non-interactive which makes the stiffness predictions conservative in a large fiber crack density region.

The dependence of COD on fiber and matrix properties, fiber content, debond length etc is described by simple fitting functions obtained from extensive FEM based parametric

analysis. FEM analysis is performed using a model which consists of three concentric cylinders: a) broken fiber; b) matrix cylinder; c) large cylinder of effective composite cylinder. The observed trends are described by simple fitting functions which with a high accuracy describe COD's of perfectly bonded and partially debonded cracks.
Simulations performed for carbon and glass fiber polymer composites show the significance of debond length on the stiffness reduction.

1. Constitutive relationships for laminates with intralaminar ply cracks in in-plane loading

1.1 Literature review

Composite laminates under service loading undergo complex combinations of thermal and mechanical loading, leading to microdamage accumulation in the plies, see Fig. 1.1. The first mode of damage is usually intralaminar cracking with the crack plane transverse to the laminate middle-plane, spanning the whole width of the specimen. The density of cracks in a ply depends on layer orientation with respect to the load direction, temperature change, number of cycles in fatigue, laminate lay-up, ply thickness and, certainly, material fracture toughness. Relative displacements of crack surfaces during loading reduce the average strain and stress in the damaged layer, thus reducing the laminate stiffness. Many papers have been written on this subject, covering a broad range from micromechanics based to continuum damage mechanics based models (see review for example in Nairn and Hu (1994), Nairn (2000) and Talreja (1994)).

Most of the research has, however, been focused on cross-ply laminates which are excellent for academic studies of phenomena but are seldom used in practical applications. Laminates with a general lay-up containing cracks in several layers of

different orientation are, therefore, a challenge for any constitutive model.

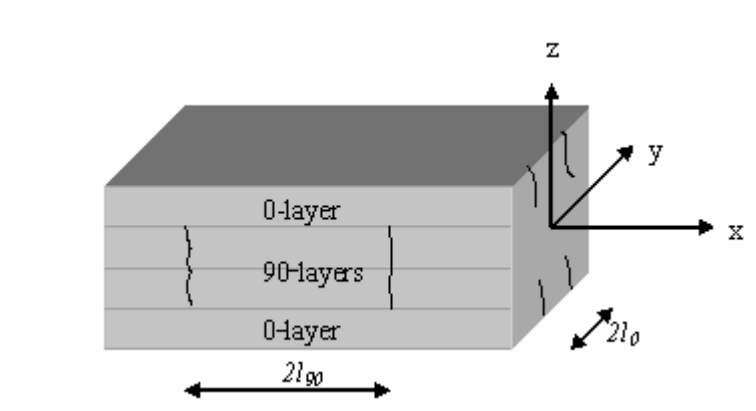

Figure 1.1. *Schematic view over $[0,90]_s$ laminate with two orthogonal systems of cracks.*

A two-dimensional shear-lag analysis is a simplest way to describe a doubly periodic matrix cracking in cross-ply laminates. It is used in Henaff-Gardin et al. (1996), where parabolic shape of the crack face is assumed to model the crack profile. It means that no distinction has been made between crack shape in the internal and the external layers. Model for general in-plane loading is derived for $[0_m,90_n]_s$ laminates averaging the equilibrium equations and obtaining second order differential equations in a usual way. Unfortunately, there is no comparison with experimental data or with other models in this paper.

Hashin (1987) generalized his model (Hashin, 1985) to the case when cracks are in both 0- and 90-layers of a cross-ply laminate. Solution for an orthogonally cracked cross-ply laminate under tension was found constructing a simple admissible stress field in the context of the principle of minimum complementary energy. The chosen stress field satisfies equilibrium equations and all boundary and interface conditions in tractions. The assumed constant in-plane normal stress distribution over each layer thickness leads to linear and parabolic through-the-thickness distributions of out-of-plane shear and normal stresses, respectively. The principle of minimum complementary energy (which for approximate stress distributions is equivalent satisfying the displacement continuity equations in average) is used to calculate the stress distributions. Expressions for

damaged laminate E-modulus and Poisson's ratio were derived. This model does not involve any fitting parameters and is simple to use. Since Hashin's model renders a lower bound of the stiffness, its accuracy could be improved by more refined assumptions regarding the thickness coordinate dependence of stresses. The assumptions used are oversimplified and give too low stiffness of the damaged laminate.

McCartney (1992) applied his model, which is based on the same stress distribution assumptions as Hashin's model (Hashin, 1987) but the governing equations are obtained from Reissners principle, to doubly-cracked cross-ply laminates assuming that the in-plane normal stress dependence on the two in-plane coordinates is given by two independent functions.

Model of similar accuracy as Hashin's and McCartney's models was developed by Abdelrahman and Nayfeh (1999) to analyze stiffness of doubly-cracked cross-ply laminates. In addition to the assumptions of a linear shear stress distribution across of each layer, which is the same as in Hashin's model, authors assume linear distribution of out-of-plane displacements. These assumptions allow for exact satisfaction of all displacement and traction interface and boundary conditions. Since in derivations only the stress-strain relationships averaged over the layer thickness are used, the constitutive relationships are not satisfied point-wise. The governing equations are a system of two 4^{th} order partial differential equations with constant coefficients. Unfortunately, predictions and comparison with test data and other models are presented only for the case of one crack system.

The most accurate local stress state comparable with a very fine FE solution and, therefore, also accurate stiffness prediction can be obtained using semi-analytical McCartney (1995) and Schoeppner and Pagano (1998) models. In the McCartney model each layer in the laminate is divided in a certain number of thin sub-layers and in each sub-layer the stress assumptions are as in Hashin's variational model (Hashin, 1985). All displacement and stress continuity conditions at sub-layer interfaces are satisfied as are the stress-strain relationships, except one, which is satisfied in an average sense. It has been shown that this "satisfying in average" is identical to minimization of the Reissner energy functional in the used approximation of the stress-strain state. The Schoeppner-Pagano model (1998), which is also based on Reissners principle, considers a system of

hollow concentric sub-cylinders with a large radius instead of laminate divided in sub-layers. Each layer is divided in a number of cylinders. In order to simulate interface cracks these cylinders may also be connected in parallel. Shape functions for each sub-cylinder in this model are different than in McCartney's model but the results converge with increasing number of sub-layers (sub-cylinders) (MC Cartney et al., 2000). However, the calculation routines in these models are extremely complex which limits the application.

Neither of these models can be directly used for laminates containing several systems of cracks. However, considering these crack systems as non-interacting one can first introduce crack system in 90-layer only and back-calculate the effective stiffness of the damaged layer from the damaged laminate stiffness. Then the intralaminar cracks are introduced in the 0-layer only and similar problem as described above is solved in a system of coordinates rotated by 90°. Finally the effective properties of all damaged layers may be used in laminate theory to calculate the stiffness of laminate with cracks in both layers. The Schoepner and Pagano model has been used in this way to predict the reduction of thermal expansion coefficients of cross-ply laminates with cracks in both 0- and 90-layers in (Kim et al., 2000).

Analytical modeling of in-plane shear modulus of the damaged laminate is considered only in a few investigations.

Hashin (1985) investigated the in-plane shear modulus reduction of cross-ply laminates with cracks in inside 90-layer using a variational approach. In his model an admissible stress field is constructed which satisfies equilibrium as well as the boundary and interface conditions in tractions. The in-plane shear stress distribution across each ply was assumed uniform and the only unknown function describing the shear stress in-plane distribution was determined using the principle of minimum complementary energy. Using the calculated stress distribution the lower bounds for the shear modulus of the laminate was obtained. Exactly the same expression for shear modulus reduction was obtained using two entirely different approaches (Nuismer et al., 1988, Tan et al., 1989, Tsai et al., 1992, 1990, Abdelrahman et al., 1999): a) Tan et al.(1988, 1989) obtained expressions for axial modulus, Poisson's ratio and shear modulus of the cross-ply laminate with 90-cracks integrating the equilibrium and constitutive expressions over the

ply thickness and obtaining a second order differential equations for stress distributions; b) Tsai et al (1990, 1992) and Abdelrahman et al (1999) reduced the 3-D elasticity problem to 2-D problem in terms of displacements (Tsai et al., 1992) or stresses (Abdelrahman et al., 1999) averaged over the ply thickness and solved analytically the obtained set of differential equations with constant coefficients. The results of all these models coincide due to assumed linear through the thickness dependence of the out-of-plane shear stresses. Henaff-Gardin et al (1996) analyzed the double-cracked cross-ply laminates in a similar manner as in Tsa et al., (1992) just using simpler shear lag model with parabolic opening displacement and uniform sliding displacement distributions. Since the free crack surface conditions were satisfied only in average, they could find the shear stress distribution analytically. Tsai et al (1992) developed a methodology for shear modulus determination using an experimental setup where a pre-damaged tensile specimen is subjected to in-plane tangential displacement in the middle part. Then the shear modulus was calculated using a Timoshenko beam approximation of the specimen deformation. Herakovich et al (1988) used for displacements in a layer of a cross-ply laminate with cracks in 90-layer a second order Legendre expansion with respect to the out-of-plane coordinate z . The set of governing equations for the 9 unknown functions of in-plane coordinates was obtained multiplying equilibrium equations by z^n and integrating, and solved using finite differences. Comparison with FEM results showed that the approximate model gives consistently too small stiffness reduction. Hua Yu et al (1996) used approach by Tsai et al. (19992) to analyze the stiffness matrix of unbalanced $[\theta_m/90_n]_s$ laminates with cracks in 90-layers by partition the initial coupled problem in two uncoupled subproblems, the first of them being exactly the same as in Tsa et al., 1992.

Tsai et al (1990) considered also shear response of cross-ply laminates with cracks in both 90- and 0-layer. In this case the set of 2-D equations was solved numerically using finite differences. They suggested that an expression based on “superposition of solutions” may give good accuracy.

Fan et al (1993), using the expressions for a compliance of a solid with microcracks derived by Horii et al (1980), presented the constitutive equations for a layer with cracks. These expressions apart from lamina properties contain also so-called “in-situ damage

effective functions -IDEF" which depend on crack density in the lamina and on the neighbouring layer constraint. In order to determine IDEF they introduced "an equivalent constraint model", which assumes that the constraint of the lay-ups above and below the analyzed lamina can be described by two sublaminates with properties calculated using laminate theory (CLT). Thereby the actual laminate was replaced by a cross-ply. The stress state in the repeating unit of the cross-ply laminate and the IDEF's were calculated using standard shear lag model with linear distribution of out-of-plane shear stresses. Then the constitutive relationships for damaged layers were used in the framework of the CLT to obtain the stiffness matrix of the damaged laminate. Since the micromechanical local stress model coincides with the presented in Tsai et al. (1990, 1992), the predictions of the shear modulus for the cross-ply laminate with cracks in 90-layer only, which is the only case discussed in Fan et al. (1993), also have to coincide or be very similar. This approach was further refined by Zhang et al (1992) where the local stress problem was solved using an improved shear lag model which assumes non-zero 0-layer intralaminar shear stress only in a zone in the vicinity of the transverse crack tip. The only problem is that the size of this zone becomes a fitting parameter.

The same micromechanics model was used also by Kashtalyan et al (2000) where in the "equivalent constraint model" the effective properties of the constraint layer were adjusted for damage when analyzing the local stresses in another layer. This leads to an iterative procedure when cracks are present in both 0- and 90-layer of the cross-ply laminate. It was shown that a) the results are quite different when the shear stress localization model is used; b) the interaction of cracks in two layers leads to considerable additional reduction of the laminate shear modulus. It should be noted that the methodology, which was developed and used for cross-ply laminates, could be rather easy generalized to more general lay-ups. Local delaminations at the tip of transverse cracks were included in the analysis by the same authors (2002) were also a rather detailed analysis of the state of art on this subject is presented.

Generally speaking, the continuum damage mechanics (CDM) approaches (Allen et al., 1987, Ladeveze, 1980, Talreja, 1994) may be used to describe the stiffness of laminates with intralaminar cracks in off-axis plies of any orientation. The damage is represented by internal state variables (ISV) and the laminate constitutive equations are expressed in

general forms containing ISV and a certain number of material constants. These constants must be determined for each considered laminate configuration either experimentally measuring stiffness for a laminate with a certain crack density or using FE analysis for the same reason. This limitation is partially removed in synergistic damage mechanics suggested by Talreja (1996) which incorporates micromechanics information to determine the material constants. For the same $[\pm\theta, 90_2]_s$ class of laminates as in theoretical assessment (Talreja, 1996). Varna et al. (1999a) used experimentally measured crack opening displacement (COD) to identify the constraint parameter in CDM and to make stiffness predictions. For these measurements a special device was designed and measurements were performed using optical microscopy on loaded specimens (Varna, 1993). The same technique was later applied to measure COD for cracks in off- axis plies of $[0/\pm\theta_4/0_{1/2}]$s laminates and to perform CDM predictions (Varna et al., 1999b).

An extensive FE parametric analysis in plane stress formulation was performed by Joffe et al. (2001) to identify the main geometrical and stiffness parameters affecting the COD. It was found that average COD normalized with respect to the far field stress in the layer and the layer thickness is a very robust parameter: variation of shear moduli and Poisson's ratios has a negligible effect on the normalized COD. Only the stiffness and thickness ratios of the cracked to uncracked neighboring layers have a significant effect. Based on numerical results the numerical COD values were fitted by power law. The main conclusion was that increasing stiffness and thickness of the constraint layer leads to significant reduction of the average normalized COD.

This power law for COD was used in the synergistic CDM predictions of stiffness reduction in $[\pm\theta,90_4]_s$ laminates (Varna et al., 2001) with cracks in 90-layers only. Recently it was demonstrated using micromechanics that all material parameters in CDM for this lay-up depend only on the material properties of the layer, not on the laminate lay-up (Varna et al., 2003). This finding was not proven for laminates with cracked layers other than 90° because analytical micromechanics solution for a general case does not exist.

Gudmundson and co-workers (1992, 1993) considered laminates with general lay-up and used homogenization technique to derive expressions for stiffness and thermal expansion

coefficient of laminates with cracks in layers of 3-D laminates. These expressions in an exact form correlate damaged laminate thermo-elastic properties with parameters characterizing crack behavior: the average COD and crack face sliding. These parameters follow from the solution of the local boundary value problem and their determination is a very complex task. Gudmundson and co-workers suggested to neglect the effect of neighboring layers on crack face displacements and to determine them using the known solution for a periodic system of cracks in an infinite homogeneous transversely isotropic medium (90-layer). The application of their methodology by other researchers has been rather limited due to the fairly complex form of the presented solutions.

In the present report an approach, similar to that performed by Gudmundson, is presented in the framework of the laminate theory. The largest advantage in this methodology is the transparency of derivations and the simplicity of application (the ideas were introduced by Lundmark and Varna, 2003, 2005, 2006). Stiffness or compliance matrices and thermal expansion coefficients of an arbitrary symmetric laminate with damage in certain layers are presented in an explicit form. Derivation of constitutive relationships follows the same route as in classical laminate theory. As an input from homogenization theory the relationships between volume averaged and boundary surface averaged quantities are used. The differences between undamaged and damaged laminate cases are indicated in each step of derivation. The damaged laminate stiffness and thermal expansion coefficients are calculated from the undamaged laminate stiffness and the crack face displacements.

In contrast to Gudmundson's approach (Gudmundson and Östlund, 1992, Gudmundson and Zang, 1993) the normalized COD and crack face sliding are considered as dependent on the position of the cracked layer (outside or inside cracks) and on the constraint of the surrounding layers in terms of their stiffness and thickness. These dependences are analyzed using FEM calculated crack opening displacement profiles in generalized plane strain formulation and presenting the results in the form of power laws.

In a special case of balanced laminates with cracks in 90-layer only, expressions for thermo-elastic properties are presented in an explicit and compact form.

1.2 Modeling stress-strain response of damaged laminates

1.2.1 Problem Formulation

In this derivation, a symmetric laminate subjected to general in-plane loading is considered, see Fig. 1.2. To exclude bending effects the laminate is assumed to be symmetric also in the damaged state (crack density is the same in layers with symmetric location with respect to the mid-plane). Only in-plane loading is considered and the intralaminar cracks are assumed to run parallel to fibers with a crack plane transverse to the laminate mid-plane and to span the whole cross-section of the layer. Laminate contains N layers of which the k-th layer is characterized by stiffness $[Q]_k$, thickness t_k and fiber orientation angle which determines the stress transformation matrix $[T]_k$ between global and local coordinates. The overbar on the matrix and vectors denotes quantities in the global coordinate system. The crack density in a layer is $\rho_k = 1/2 l_k$ and normalized crack density ρ_{kn} is defined as $\rho_{kn} = t_k \rho_k$. The geometry of the problem for particular case of a doubly cracked cross-ply laminate can be seen in Fig. 1.1.

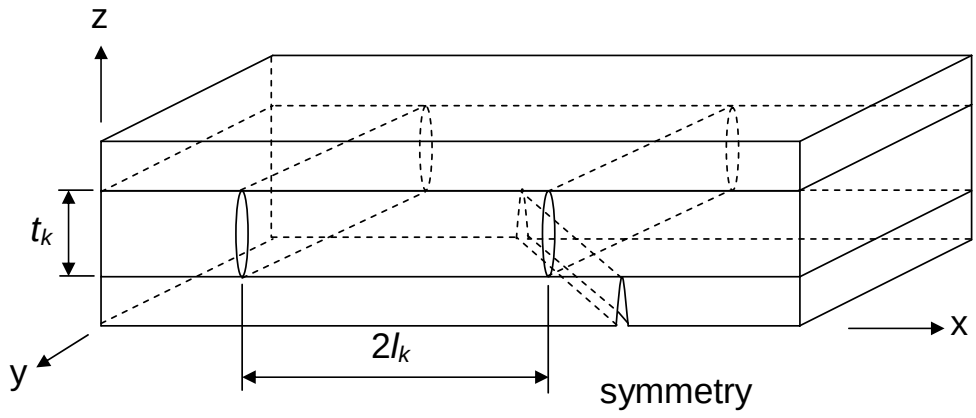

***Figure 1.2**. Geometry of RVE used in derivation*

The thermo-elastic relation between applied stresses and the strains experienced by the damaged laminate can be written in the following way.

$$\{\sigma\}^{LAM} = [Q]^{LAM}\left[\{\varepsilon\}^{LAM} - \{\alpha\}^{LAM}\Delta T\right] \tag{1.1}$$

where $$\Delta T = T - T_{ref} \tag{1.2}$$

In (1.1) $\{\sigma\}^{LAM}$ and $\{\varepsilon\}^{LAM}$ are macroscopic stress and strain vectors applied at the boundary of the representative volume element (RVE), $[Q]^{LAM}$ and $\{\alpha\}^{LAM}$ are the unknown stiffness matrix and thermal expansion coefficient vector of the damaged laminate to be determined.

1.2.2 Homogenization Relationships

Introducing volume averaged stresses and strains as in Allen et al., (1998) and using superscript *a* to denote average quantities, we have,

$$\sigma_{ij}^{a} = \frac{1}{V}\int_{V}\sigma_{ij}\,dV \qquad\qquad \varepsilon_{ij}^{a} = \frac{1}{V}\int_{V}\varepsilon_{ij}\,dV \tag{1.3}$$

Here V is the volume of averaging, which may be one layer or the whole laminate volume, as needed. The average stress-strain relationships for a *k*-th layer in the global coordinate system are

$$\{\bar{\sigma}\}_{k}^{a} = [\bar{Q}]_{k}\left[\{\bar{\varepsilon}\}_{k}^{a} - \{\bar{\alpha}\}_{k}\Delta T\right] \tag{1.4}$$

Using divergence theorem it may be shown Allen et al., (1998), Varna (2002) that stresses applied to the laminate boundary are equal to the stresses averaged over the volume of the whole laminate. Expressing the volume integral as a sum of integrals over volume of individual layers, we obtain

$$\{\sigma\}^{LAM} = \{\overline{\sigma}\}^{a} = \sum_{k=1}^{N} \{\overline{\sigma}\}_{k}^{a} \frac{t_k}{h} \tag{1.5}$$

Using the divergence theorem it can also be shown (Allen et al., 1998, Varna, 2002) that the volume average strains in each layer are equal to boundary averaged strains defined as

$$\mathrm{E}_{ij} = \frac{1}{V} \int_{S} \frac{1}{2}\left(u_i n_j + u_j n_i\right) dS \tag{1.6}$$

Definition (1.6) is written for tensorial boundary averaged strains. Using this definition one can easily check that average strains at the external boundary of a layer are equal to the applied macroscopic strains, which are the same for all layers in the damaged laminate (iso-strain condition in laminate theory).

Since the integration in (1.6) involves the total boundary including the crack surface, the abovementioned equality of volume averaged and boundary averaged strains for *k*-th layer may be written as

$$\begin{Bmatrix} \overline{\varepsilon}_1 \\ \overline{\varepsilon}_2 \\ \overline{\gamma}_{12} \end{Bmatrix}_k^a = \begin{Bmatrix} \varepsilon_1 \\ \varepsilon_2 \\ \gamma_{12} \end{Bmatrix}^{LAM} + \begin{Bmatrix} \overline{\beta}_{11} \\ \overline{\beta}_{22} \\ 2\overline{\beta}_{12} \end{Bmatrix}_k^a . \tag{1.7}$$

Here $\{\overline{\beta}\}_k^a$ is the Vakulenko-Kachanov tensor defined by

$$\overline{\beta}_{ij}^{a} = \frac{1}{V} \int_{S_C} \frac{1}{2}\left(u_i n_j + u_j n_i\right) dS \tag{1.8}$$

We will use in this paper engineering strains and engineering form of the Vakulenko-Kachanov tensor $\{\overline{\beta}\}_k$. In layers with no cracks, β_{ij} is zero. S_c is the total surface of cracks in the layer, u_i are displacements of the points on the crack surface, n_i is outer normal to the crack surface, V is the volume of the layer.

1.2.3 Crack Face Relative Displacements and Vakulenko-Kachanov Tensor

Considering (1.8) in the local co-ordinate system related to fiber orientation in the *k*-th layer, it is seen that the only non-zero components are β_{12} and β_{22} (1 is the fiber direction and 2 is transverse to the fiber direction), given by,

$$\beta_{12}^k = -\rho_k u_{1a}^k \qquad \beta_{22}^k = -2\rho_k u_{2a}^k \tag{1.9}$$

Here u_{1a}^k and u_{2a}^k are the average crack face sliding displacement and average crack face opening displacement, respectively defined as

$$u_{1a}^k = \frac{1}{2t_k}\int_{-\frac{t_k}{2}}^{\frac{t_k}{2}} \Delta u_1(x_3)\,dx_3 \qquad u_{2a}^k = \frac{1}{2t_k}\int_{-\frac{t_k}{2}}^{\frac{t_k}{2}} \Delta u_2(x_3)\,dx_3 \tag{1.10}$$

Here Δu_i are the separation distances of the two crack faces. Normalizing the displacements with respect to thickness of the cracked layer (length of the crack) and the far field (CLT) stresses in the layer corresponding to the same load applied to undamaged laminate (indicated by subscript $_0$) gives:

$$u_{1an}^k = u_{1a}^k \frac{E_2}{t_k \sigma_{120}^k} \qquad u_{2an}^k = u_{2a}^k \frac{E_2}{t_k \sigma_{20}^k} \tag{1.11}$$

Using Equation (1.11) in Equation (1.9) provides expressions for components of Vakulenko-Kachanov tensor through normalized displacements and far field stresses:

$$\beta_{12}^k = -\rho_{kn} u_{1an}^k \frac{\sigma_{120}}{E_2} \qquad \beta_{22}^k = -2\rho_{kn} u_{2an}^k \frac{\sigma_{20}}{E_2} \tag{1.12}$$

Introducing the displacement matrix U makes it possible to express the Vakulenko-Kachanov tensor in the Voigt notation as a matrix product

$$[U]_k = 2\begin{bmatrix} 0 & 0 & 0 \\ 0 & u_{2an}^k & 0 \\ 0 & 0 & u_{1an}^k \end{bmatrix} \tag{1.13}$$

$$\{\beta\}_k = -\frac{\rho_{kn}}{E_2}[U]_k \{\sigma_0\}_k \tag{1.14}$$

From here on the vectorial representation of the Vakulenko-Kachanov tensor is used.

Transforming Equation (1.14) to global coordinates is same as engineering strain transformation in CLT.

$$\{\bar{\beta}\}_k = [T]_k^T \{\beta\}_k \tag{1.15}$$

The far field stress components in the cracked layer required in Equation (1.14) can be expressed using CLT.

$$\{\sigma_0\}_k = [T]_k [\bar{Q}]_k \left[\{\varepsilon_0\}^{LAM} - \{\bar{\alpha}\}_k \Delta T \right] \tag{1.16}$$

Substituting Equation (1.16) and (1.14) in Equation (1.15) gives:

$$\{\bar{\beta}\}_k = \frac{-\rho_{kn}}{E_2} [T]_k^T [U]_k [T]_k [\bar{Q}]_k \left[\{\varepsilon_0\}^{LAM} - \{\bar{\alpha}\}_k \Delta T \right] \tag{1.17}$$

1.2.4 Constitutive Relationships for Damaged Laminates

Substituting the expression (1.7) in the averaged stress-strain relationships (1.4) and using Equation (1.5) gives the following expression for laminate stresses.

$$\{\sigma\}^{LAM} = [Q_0]^{LAM} \{\varepsilon\}^{LAM} - \frac{1}{h} \sum_{k=1}^{N} [\bar{Q}]_k \{\bar{\alpha}\}_k \Delta T \, t_k + \frac{1}{h} \sum_{k=1}^{N} [\bar{Q}]_k \{\bar{\beta}\}_k \, t_k \tag{1.18}$$

The second term on the right-hand-side of (1.18) can be identified with the "thermal force" per unit thickness, $\{\sigma\}_{th}^{LAM}$ known in laminate theory. Since it can be related to the strain response of undamaged laminate as

$$\{\sigma\}_{th}^{LAM} = [Q_0]^{LAM} \{\varepsilon_0\}_{th}^{LAM}, \tag{1.19}$$

Equation (1.18) can be rewritten in form

$$\{\sigma\}^{LAM} = [Q_0]^{LAM}\left[\{\varepsilon\}^{LAM} - \{\varepsilon_0\}_{th}^{LAM}\right] + \frac{1}{h}\sum_{k=1}^{N}[\overline{Q}]_k \{\overline{\beta}\}_k t_k \tag{1.20}$$

Here $[Q_0]^{LAM}$ is the stiffness matrix of the undamaged laminate calculated as in the classical laminate theory (CLT). $\{\varepsilon_0\}^{LAM}$ is the strain in the undamaged laminate corresponding to the same applied load $\{\sigma\}^{LAM}$.

Substituting Equation (1.17) in Equation (1.20) gives the final form for damaged laminate thermo-mechanical stress – strain response:

$$\begin{aligned}\{\sigma\}^{LAM} = [Q_0]^{LAM}&\left[\{\varepsilon\}^{LAM} - \{\varepsilon_0\}_{th}^{LAM}\right] - \\ &\frac{1}{hE_2}\sum_{k=1}^{N}\rho_{kn}\left[\overline{Q}\right]_k [T]_k^T [U]_k [T]_k \left[\overline{Q}\right]_k \left[\{\varepsilon_0\}^{LAM} - \{\overline{\alpha}\}_k \Delta T\right] t_k\end{aligned} \tag{1.21}$$

1.2.5 Stiffness and Compliance Matrices of the Damaged Laminate

Assuming only mechanical loading ($\Delta T = 0$) in equation (1.21) and using

$$\{\varepsilon_0\}^{LAM} = [S_0]^{LAM}\{\sigma\}^{LAM} \tag{1.22}$$

gives

$$\begin{aligned}\{\sigma\}^{LAM} = [Q_0]^{LAM}&\{\varepsilon\}^{LAM} \\ &-\frac{1}{hE_2}\sum_{k=1}^{N}\rho_{kn}\left[\overline{Q}\right]_k [T]_k^T [U]_k [T]_k \left[\overline{Q}\right]_k [S_0]^{LAM}\{\sigma\}^{LAM} t_k\end{aligned} \tag{1.23}$$

Expressing laminate stress from Equation (1.23) gives:

$$\{\sigma\}^{LAM} = \left([I] + \frac{1}{hE_2}\sum_{k=1}^{N}\rho_{kn}\left[\overline{Q}\right]_k [T]_k^T [U]_k [T]_k \left[\overline{Q}\right]_k [S_0]^{LAM} t_k\right)^{-1} [Q_0]^{LAM}\{\varepsilon\}^{LAM} \tag{1.24}$$

where $[I]$ is the identity matrix.

Comparing (1.24) with Equation (1.1), with $\Delta T = 0$, the stiffness matrix and corresponding compliance matrix for the damaged laminate are found to be

$$[Q]^{LAM} = \left([I] + \frac{1}{hE_2} \sum_{k=1}^{N} \rho_{kn} \left[\overline{Q}\right]_k [T]_k^T [U]_k [T]_k \left[\overline{Q}\right]_k [S_0]^{LAM} t_k \right)^{-1} [Q_0]^{LAM} \tag{1.25}$$

$$[S]^{LAM} = [S_0]^{LAM} \left([I] + \frac{1}{hE_2} \sum_{k=1}^{N} \rho_{kn} \left[\overline{Q}\right]_k [T]_k^T [U]_k [T]_k \left[\overline{Q}\right]_k [S_0]^{LAM} t_k \right) \tag{1.26}$$

These expressions may be used to calculate the degradation of mechanical properties for the damaged laminate.

1.2.6 Thermal Expansion Coefficients of the Damaged Laminate

If the reductions in thermal properties are of interest a derivation based on thermal loading only has to be done. Applying thermal loads only, the global laminate stresses are equal to zero, and Equation (1.20) allows determining the thermal expansion strains of the damaged laminate.

$$\{\varepsilon\}^{LAM} = \{\varepsilon_0\}_{th}^{LAM} - [S_0]^{LAM} \frac{1}{h} \sum_{k=1}^{N} \left[\overline{Q}\right]_k \left\{\overline{\beta}\right\}_k t_k \tag{1.27}$$

Applying Equation (1.17) in (1.27), the following relationship can be obtained.

$$\begin{aligned} \{\varepsilon\}^{LAM} = \{\varepsilon_0\}_{th}^{LAM} + [S_0]^{LAM} \frac{1}{hE_2} \sum_{k=1}^{N} \rho_{kn} \left[\overline{Q}\right]_k [T]_k^T [U]_k [T]_k \left[\overline{Q}\right]_k \{\varepsilon_0\}_{th}^{LAM} t_k - \\ [S_0]^{LAM} \frac{1}{hE_2} \Delta T \sum_{k=1}^{N} \rho_{kn} \left[\overline{Q}\right]_k [T]_k^T [U]_k [T]_k \left[\overline{Q}\right]_k \left\{\overline{\alpha}\right\}_k t_k \end{aligned} \tag{1.28}$$

By dividing Equation (1.28) by ΔT, the final expression for the thermal expansion coefficient for the damaged laminate is obtained.

$$\{\alpha\}^{LAM} = \left([I] + \sum_{k=1}^{N} \frac{t_k}{h} \rho_{kn} [D]_k \right) \{\alpha\}_0^{LAM} - \sum_{k=1}^{N} \frac{t_k}{h} \rho_{kn} [D]_k \{\bar{\alpha}\}_k \tag{1.29}$$

where

$$[D]_k = [S]_0^{LAM} \frac{1}{E_2} [\bar{Q}]_k [T]_k^T [U]_k [T]_k [\bar{Q}]_k \tag{1.30}$$

1.3 Thermo-Elastic Properties of Laminates with Cracks in 90-layers

In balanced and symmetric laminates with cracks in 90-layers only the matrix relationships for stiffness and thermal expansion coefficients may be simplified and expressed in explicit form. We consider a particular case often used in research when the 90-layer with crack density ρ_n is in the middle of the laminate. The set of layers surrounding the 90-layer on either side may be considered as a sublaminate with thermo-elastic properties calculated using CLT and denoted by upper index s. Using 90-layer properties in the local system and denoting thickness of the sublaminate and 90-layer by t_s and t_{90}, respectively, we obtain, after tedious work, the following relationships for engineering constants of the damaged laminate.

$$\frac{E_x}{E_{x0}} = \frac{1}{1 - Q_{22}(1 - \upsilon_{12}\upsilon_{xy0}) g_3 k \rho_n u_{2an}} \tag{1.31}$$

$$\frac{E_y}{E_{y0}} = \frac{1}{1 - Q_{22} \frac{(\upsilon_{12} - \upsilon_{yx0})^2}{1 - \upsilon_{12}\upsilon_{xy0}} \frac{\upsilon_{xy0}}{\upsilon_{yx0}} g_3 k \rho_n u_{2an}} \tag{1.32}$$

$$\frac{\upsilon_{xy}}{\upsilon_{xy0}} = \frac{1 + Q_{22}\left(\frac{\upsilon_{12} - \upsilon_{yx0}}{\upsilon_{yx0}}\right) g_3 k \rho_n u_{2an}}{1 - Q_{22}\left(1 - \upsilon_{12}\upsilon_{xy0}\right) g_3 k \rho_n u_{2an}} \tag{1.33}$$

$$\frac{\upsilon_{yx}}{\upsilon_{yx0}} = \frac{1 + Q_{22}\left(\frac{\upsilon_{12} - \upsilon_{yx0}}{\upsilon_{yx0}}\right) g_3 k \rho_n u_{2an}}{1 - Q_{22}\frac{\left(\upsilon_{12} - \upsilon_{yx0}\right)^2}{1 - \upsilon_{12}\upsilon_{xy0}}\frac{\upsilon_{xy0}}{\upsilon_{yx0}} g_3 k \rho_n u_{2an}} \tag{1.34}$$

$$\frac{\alpha_x}{\alpha_{x0}} = 1 - Q_{22}\frac{\left[\alpha_{x0} - \alpha_2 + \upsilon_{12}\left(\alpha_{y0} - \alpha_1\right)\right]}{\alpha_{x0}} g_3 k \rho_n u_{2an} \tag{1.35}$$

$$\frac{\alpha_y}{\alpha_{y0}} = 1 - Q_{22}\frac{\left[\alpha_{x0} - \alpha_2 + \upsilon_{12}\left(\alpha_{y0} - \alpha_1\right)\right]}{\alpha_{y0}}\frac{\left(\upsilon_{12} - \upsilon_{yx0}\right)}{1 - \upsilon_{12}\upsilon_{xy0}}\frac{\upsilon_{xy0}}{\upsilon_{yx0}} g_3 k \rho_n u_{2an} \tag{1.36}$$

where

$$g_3 = \frac{t_{90}}{2t_s}\left(S^s_{xy}\frac{S_{12}t_s + S^s_{xy}t_{90}/2}{S_{11}t_s + S^s_{yy}t_{90}/2} - S^s_{xx}\right) \tag{1.37}$$

$$\frac{1}{k} = \frac{E_2 t_{90}}{4E^s_x t_s}\left[1 + \frac{2S_{22}t_s}{S^s_{xx}t_{90}} - \frac{2\left(S^s_{xy}t_{90}/2 + S_{12}t_s\right)^2}{S^s_{xx}t_{90}\left(S^s_{yy}t_{90}/2 + S_{11}t_s\right)}\right] \tag{1.38}$$

In (1.37) and (1.38) S_{ij} are elements of the compliance matrices. In particular case of cross-ply laminate, the sublaminate is the 0-layer, and,

$$S^s_{xx} = S_{11}, \quad S^s_{yy} = S_{22}, \quad S^s_{xy} = S_{12}, \quad E^s_x = E_1 \tag{1.39}$$

Expression for $Q^{LAM}_{66} = G_{xy}$ of $[S,90_n]_s$ and $[90_n,S]_s$ laminates with cracks in 90-layer may be written in the following form

$$\frac{G_{xy}}{G_{xy}^0} = \frac{1}{1 + \dfrac{2G_{12}t_{cr}}{G_{12}t_{cr} + G_{xy}^s t_s}\rho_n u_{1an}} \tag{1.40}$$

In this particular case only the CSD enters the expression for shear modulus.

Equation (1.40) is valid for both "inside cracks" (use $t_{cr} = t_{90}/2$, see Fig. 1.5 a)) and for "outside cracks" ($t_{cr} = t_{90}$, see Fig.1.5b)). We call a crack an inside crack if the cracked layer does not have a free surface and outside crack if it has a free surface. Certainly, u_{1an} defined by equations (1.10), (1.11) may be different for both types of cracks.

For a cross-ply laminate with cracks in 90-layer only (the sublaminate is the 0-layer), the shear modulus can be expressed as

$$\frac{G_{xy}}{G_{xy}^0} = \frac{1}{1 + 2\rho_n \dfrac{t_{90}}{t_{90} + 2t_s} u_{1an}} \tag{1.41}$$

1.4 Crack opening (COD) and sliding (CSD) displacements

The normalized COD and CSD of a crack in a cracked layer of a general laminate are affected by the material and geometrical properties of the materials surrounding the crack. For the COD case it was shown previously by Joffe et al., (2001) that u_{2an} is a rather robust parameter and its value depends only on the stiffness ratio and thickness ratio of the constraining and cracked layers. Since it was possible to express this relationship in a form of a simple power law, this finding significantly simplified the laminate stiffness prediction procedure for cases when the COD is the governing parameter and the CSD may be neglected. The approach is actually similar to the "equivalent constraint model" described by Fan et al., (1993): In order to calculate the u_{2an} of a crack in the local axes, where the cracked layer has a 90-orientation, we consider an artificial cross-ply laminate with layer properties as for the cracked- and the closest constraining layer and determine the COD using the power law. In this paper the

objective is to investigate the parameters affecting the CSD and to describe the dependence by simple expression.

FE calculations were used to perform parametric analysis of the main factors governing the value of the normalized crack opening and sliding displacements; For all FE calculations the commercial code ANSYS 9.1 was used. In order to model the repeating volume element (see Figure 1.3), a 3-D model was created. The SOLID185 elements were used in all calculations. The main motivation for choosing a 3-D model was to use the same elements for all 3-D calculations (two orthogonal crack systems) and for generalized plain strain case (one system of cracks).

Analyzing crack opening COD two geometrical configurations were considered; see Fig. 1.3 for geometry and boundary conditions modeled. In the first the cracked layer is in the middle of the laminate (*inside* crack) and in the second case the crack is in the surface layer (*outside* crack). The upper boundary of the laminate was always traction free. Analyzing the COD the crack density was always chosen small enough to get non-interacting cracks ($2l_0/t_{90} = 5$ for *inside* cracks) and the number of elements was 6400. Analysis of crack interaction was left for later. The stiffness ratio between the sub-laminate and 90-layer as well as the layer thickness ratio were varied. Fig. 1.3 represents a quarter of the RVE defined in Fig. 1.1. For more detailed analysis and parameter study using plane stress formulation, see Joffe et al., (2001). For *outside* crack, the sub-laminate and 90-layer have interchanged places.

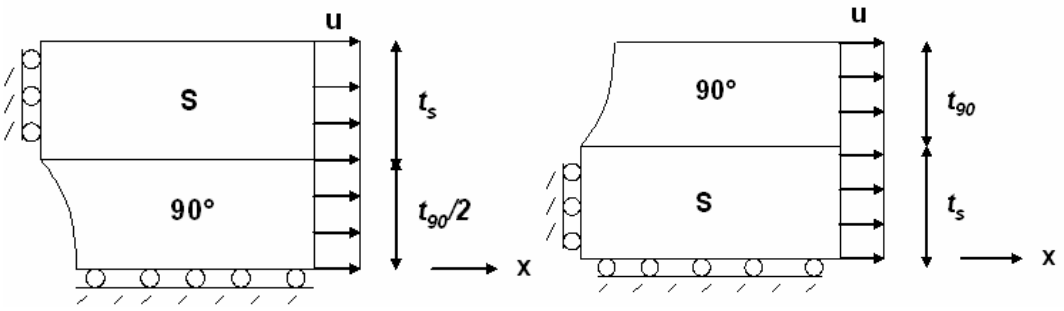

Figure 1.3. *Load cases used for determination of average crack face opening displacement.*

Calculating the crack face sliding displacements the commercial code ANSYS 11.1 was used. Since symmetry is applied on the surface z = 0, see Fig. 1.5, 3D model was created that corresponds to the upper half of the real RVE containing one crack in 90-layer. The boundary conditions applied to the RVE can be seen in Fig. 1.6. The top and bottom surfaces $z = \pm h/2$ are traction-free. Tangential displacements are applied to the side surfaces (edges). The relationship $u_{y0}/2l_{90}=u_{x0}/w$ and displacement coupling were applied. It means that points on the surface at y=-w has the same displacement in z and y-direction as the corresponding points on the surface at y=0. In the same way the points on the surfaces at x=-l_{90} and x=l_{90} have the same displacement in z and x-direction. The 3-D 8-node structural solid element SOLID185 with three degrees of freedom for each node was used and the number of elements was 21000. At first, a series of calculations were performed changing the distance between two cracks to see when the cracks start to be non-interactive. The condition for non-interacting cracks was that the in-plane shear stress was constant with respect to z at y=-w/2, x=l_{90} in the coordinate system in Fig. 1.5 and 1.6.

1.4.1 Determination of Constants in Power Law for COD

In this work, the normalized crack face opening displacement introduced in Equations (1.10), (1.11) is fitted by a power law as follows.

$$u_{2an} = A + B\left(\frac{E_2}{E_x^s}\right)^n \tag{1.42}$$

This implies that in-log-log axes there is a linear relationship

$$\log(u_{2an} - A) = \log B + n\log\left(\frac{E_2}{E_x^s}\right) \tag{1.43}$$

A series of FEM-calculations were performed and shown the relationship is rather linear for all possible combinations of geometrical and other material parameters. FEM data were used to determine the constants in Equation (1.42). The displacement in x-direction for the nodes at the crack surface was used to calculate the average value of the crack face displacement, u_{2a}. That value was then normalized with respect to thickness of the cracked layer and the far field stress in the layer transverse to the crack plane according to Equation (1.12). The obtained constants are different dependent on the position of the cracked layer. The two power laws for *inside* and *outside* cracks respectively are given below.

For *inside* crack:

$$A = 0.52$$

$$B = 0.3075 + 0.1652\left(\frac{t_{90} - 2t_s}{2t_s}\right)$$

$$n = 0.030667\left(\frac{t_{90}}{2t_s}\right)^2 - 0.0626\left(\frac{t_{90}}{2t_s}\right) + 0.7037 \qquad (1.44)$$

For *outside* crack:

$$A = 1.2$$

$$B = 0.5942 + 0.1901\left(\frac{t_{90} - 2t_s}{2t_s}\right)$$

$$n = -0.13073\left(\frac{t_{90}}{2t_s}\right)^2 + 0.4437\left(\frac{t_{90}}{2t_s}\right) + 0.2576 \qquad (1.45)$$

The normalized COD's for *inside* and *outside* cracks versus layer stiffness ratio in case of [S,90]s and [90,S]s laminate is shown in Fig. 1.4. Both, directly calculated by FEM and from the power law are in a very good agreement: the power law gives a very good description of the COD's for both crack systems. The normalized COD of the outside crack is significantly larger and both crack types show strong dependence of COD on the surrounding layer thickness. The increasing constraint due to stiffer surrounding layers may lead to 30% reduction of the COD as compared to crack surrounded by an isotropic medium. The values corresponding to solution for a periodic system of cracks in an infinite transversally isotropic medium used in Gudmundson et al. (1993) are also shown

for comparison. Obviously, they do not depend either on the relative stiffness of layers nor on their thickness. The thickness of the constraint layer has a similar effect as its stiffness: increase leads to smaller normalized COD.

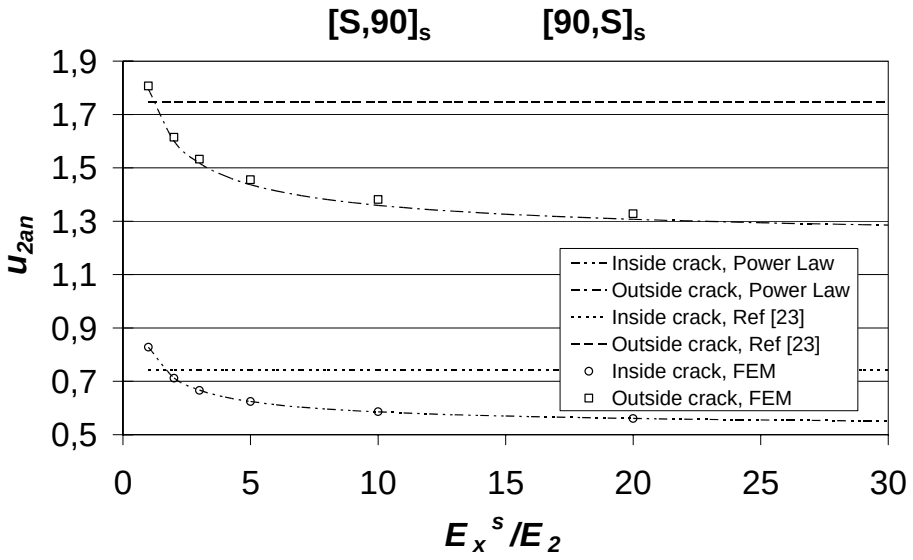

Figure 1.4. *The dependence of the normalized crack face opening displacement u_{2an} on the layer stiffness ratio for both inside($[S,90]_s$ $2t_s=t_{90}$) and outside crack($[90,S]_s$ $t_s=t_{90}$) . Fitting by power law (PL).*

1.4.2 Determination of parameters in power law for crack face sliding displacement CSD

The two geometries used in parametric studies are shown in Fig 1.5.

We found u_{1an} by calculating the sliding displacement u_y distribution along the z-coordinate at the crack surface by FEM and determining the average sliding displacement using equation (1.10). Then equation (1.11) was used for normalization.

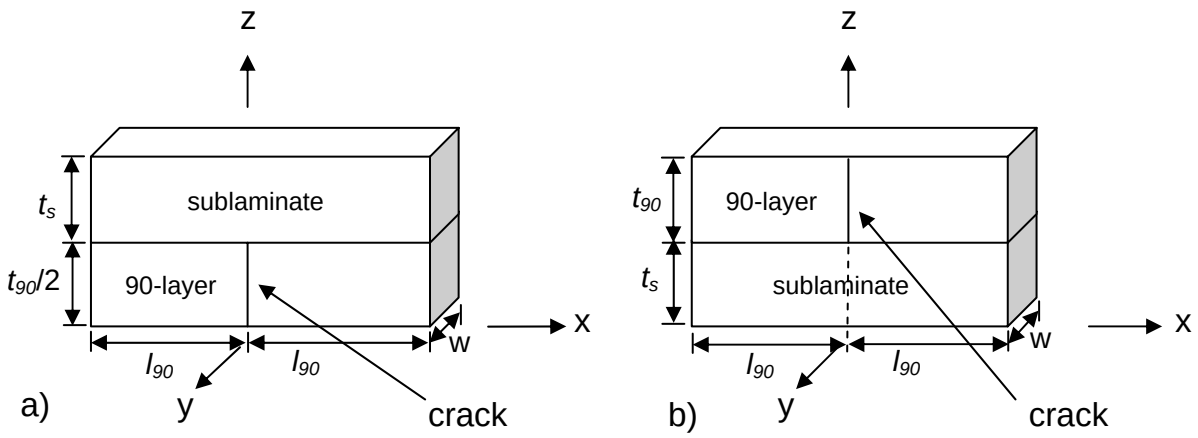

Figure 1.5. *FE-models for calculation of sliding and corresponding shear modulus.*

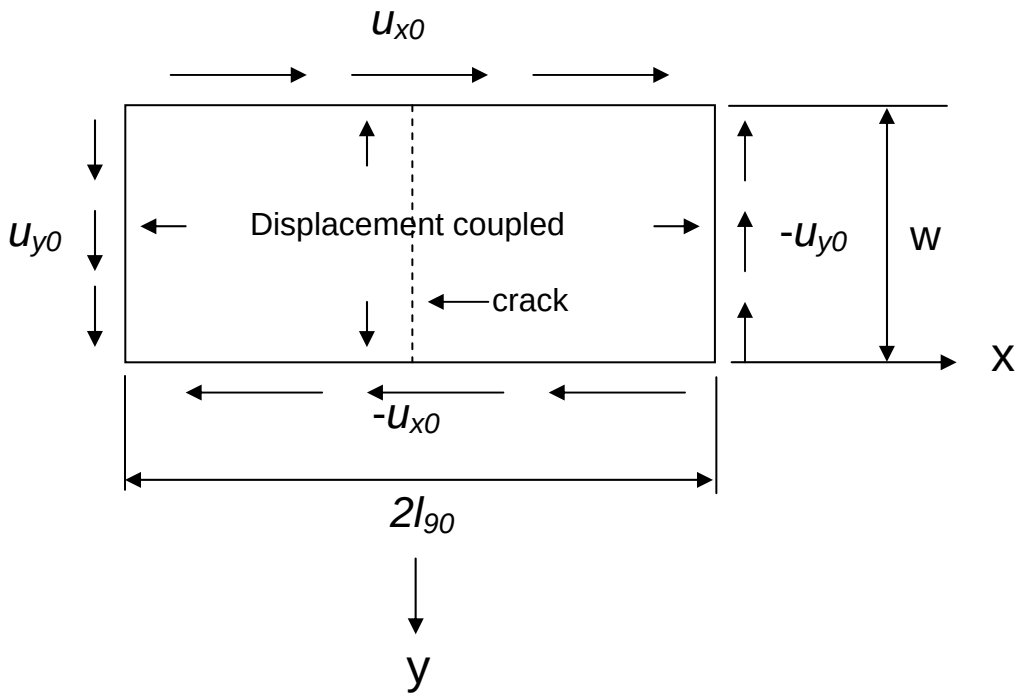

Figure 1.6. *Top view: Applied boundary conditions used for pure shear modelling.*

The three different materials used in the parametric analysis and in simulations (next section) are defined in Table 1.1.

Table 1.1. *Material properties used in calculations.*

material	E_1 (GPa)	E_2 (GPa)	υ_{12}	υ_{23}	G_{12} (GPa)	G_{23} (GPa)	Lamina thickness (mm)
GF/EP	45.0	15.0	0.30	0.40	5.00	5.36	0.100
CF/EP-1	137.0	8.39	0.38	0.47	8.04	2.85	0.132
CF/EP-2	145.0	10.6	0.27	0.40	6.90	3.70	0.100

To start with, all parameters that affect the sliding displacement were found. This was done in a series of FE-calculations changing the material parameters and geometry and calculating the laminate shear modulus. This is an indirect method of finding the parameters that affects the sliding, i.e no change in shear modulus implies no change in the CSD. The obtained results for a $[0_2,90_2]_s$ laminate with inside cracks are given in Table 1.2 below.

Table 1.2. *Results from parametric study for $[0_2,90_2]_s$ laminate, ρ= 0.25 cracks/mm*.

E_1 (GPa)	$\boldsymbol{G_{xy}}$ (GPa)		E_2 (GPa)	$\boldsymbol{G_{xy}}$ (GPa)		υ_{12}	$\boldsymbol{G_{xy}}$ (GPa)		υ_{23}	$\boldsymbol{G_{xy}}$ (GPa)		G_{23} (GPa)	$\boldsymbol{G_{xy}}$ (GPa)
20	**4.803**		10	**4.803**		0.20	**4.803**		0.25	**4.803**		4	**4.799**
30	**4.803**		20	**4.803**		0.35	**4.803**		0.35	**4.803**		5	**4.802**
60	**4.803**		30	**4.804**		0.40	**4.803**		0.55	**4.803**		6	**4.805**

The parametric study shows that only the in-plane shear modulus ratio between the sub-laminate and the 90-layer and the ratio $t_{90}/2t_s$ has influence on the in-plane shear modulus of the laminate and on the CSD. All other stiffness ratios and Poisson's ratios between the 90-layer and the sub-laminate do not influence the reduction in the in-plane shear modulus.

Then the effect of the significant parameters was quantified. To simplify the semi-empirical expression for the CSD which is obtained based on these results, the

consideration was limited to cracks in a layer which are non-interactive. This means that the distance between the cracks was large enough to avoid the stress-perturbations from two neighboring cracks in the same layer to overlap. A consequence may be a decreased accuracy of predictions (still conservative) at large crack densities.

The crack density ($2l_{90}/t_{90}=10$) was defined as non-interactive based on these calculations and used in the parametric study where the material properties and geometry were changed. The crack related stress perturbation region slightly decreases with increasing shear modulus and thickness of the constraint layer. The chosen non-interactive crack density insures that cracks are non-interactive in the used region of parameters.

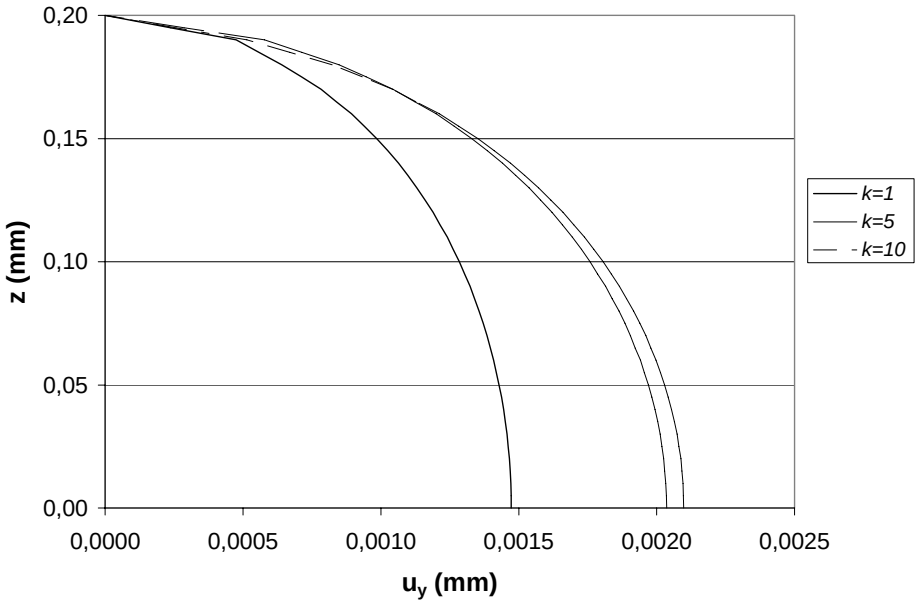

***Figure 1.7**. Sliding displacement profile for GF/EP $[0_2,90_2]_s$ laminate at 1% applied shear strain, $k = 2l_{90}/t_{90}$.*

The profile of the crack surface sliding displacements can be seen in Fig. 1.7 for a GF/EP $[0_2,90_2]_s$ laminate for three different crack densities and y=-*w*/2. Indeed, with increasing distance between cracks the sliding displacement approaches to an asymptotic value characterizing non-interactive cracks.

In Fig. 1.8 the sublaminate S_n has properties of 0-layer of GF/EP in Table 1.1 excluding the in-plane shear modulus which is used as a variable parameter.

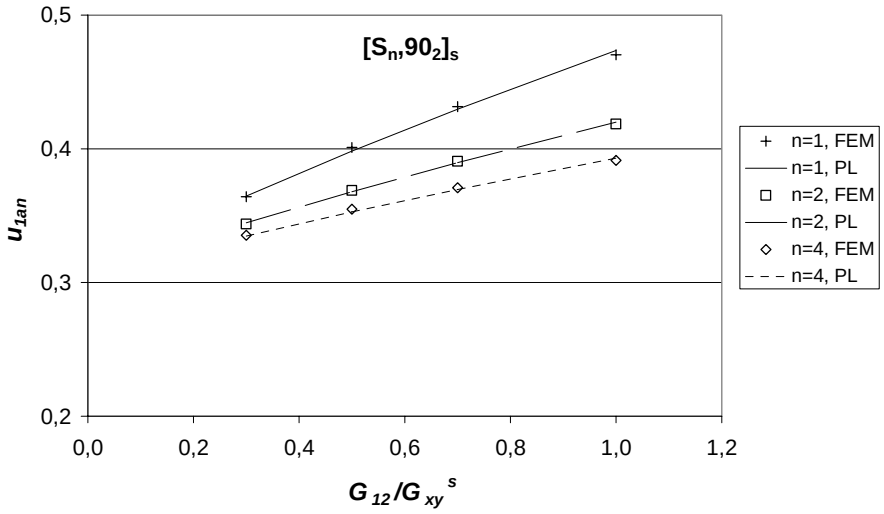

Figure 1.8a. *The power law (PL) compared with direct FE-calculations for GF/EP with inside cracks.*

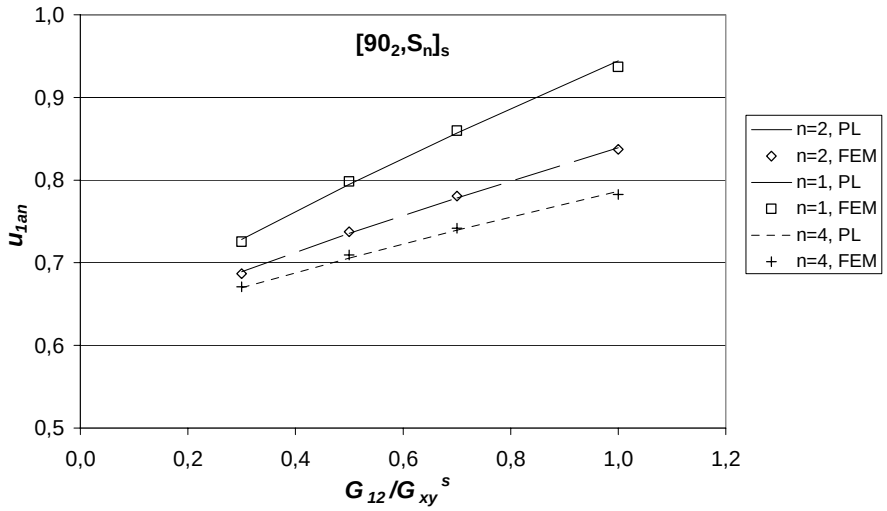

Figure 1.8b*. The power law (PL) compared with direct FE-calculations for GF/EP with outside cracks.*

The dependence of the CSD in Fig. 1.8 on shear modulus of the sublaminate is rather smooth and the values are rather different for inside and outside cracks. A general

observation is that the CSD decreases with increasing shear modulus and thickness of the constraining layer. The dependence on the modulus ratio is almost linear.
The reference set of material parameters is as for GF/EP, which means that only one property is changed at the same time while the other properties are as for GF/EP. The results of the parametric study indicate that a simple and sufficiently accurate expression for u_{1an} as a function of G_{12}/G_{xy}^{s} and $t_{90}/2t_s$ may be found thereby avoiding time-consuming FE-calculations.

The following power law expression was obtained in attempts to fit the normalized average crack face sliding displacement data presented in Fig. 1.8. The fit is based on the FEM results for non-interacting cracks ($2l_{90}/t_{90} = 10$).

$$u_{1an} = \left[A + B\left(\frac{G_{12}}{G_{xy}^{s}} \right)^{n} \right] \tag{1.46}$$

Applying a linear fit to the calculated u_{1an} versus stiffness ratio data in log-log axes gives the values of the parameters A, B and n. It was found that A and n can be approximated by constants and B by a linear function of thickness ratio for both inside and outside cracks.

-Inside cracks

$$\begin{aligned} A &= 0.3 \\ B &= 0.066 + 0.054\left(\frac{t_{90}}{2t_s} \right) \\ n &= 0.82 \end{aligned} \tag{1.47}$$

-Outside cracks

$$A = 0.6$$
$$B = 0.134 + 0.105\left(\frac{t_{90}}{t_s}\right) \qquad (1.48)$$
$$n = 0.82$$

According to (1.46), (1.47), (1.48) the normalized average CSD of, for example, $[0,90]_s$ cross-ply laminate is almost exactly two times smaller than for $[90,0]_s$ laminate which has the same total thickness of the 90-layers and 0-layers. However, according to (1.15) the effect of one crack on the laminate shear modulus is almost the same in both laminates: the calculated CSD is multiplied in equations (1.40), (1.41) by the **normalized** crack density which is for the same crack spacing two times larger in $[0,90]_s$ laminate.

According to Fig. 1.8a and 1.8b the accuracy of the power law for different laminate lay-ups and used shear modulus values for sub-laminate is very good. The shear modulus of the constraining sublaminate is usually not less than the one of the 90-layer. This is the reason why the interval of the shear stiffness ratio <1 is used for determination of the parameters in the power law. An exception is a cross-ply laminate with damaged 0-layer. To see whether the power law is still applicable it was compared with FE-calculation when the shear modulus ratio $G_{12}/G_{xy}^{s} = 2$ and the difference was around 4 %. This seems acceptable due to the fact that it is an extreme situation and that a change in sliding of 4% gives a change in shear modulus less then 1 %.

1.5 Validation of the analytical simulation tool

1.5.1 Validation using FEM results regarding the thermo-elastic properties of damaged laminates

FE calculations were used to render data for validation of the developed analytical model for thermo-mechanical properties of laminates with intralaminar cracks.

In predictions for damaged cross-ply laminates the expressions in matrix form for damaged laminate stiffness (1.25) and thermal expansion coefficients (1.29), (1.30) were used along with power law expressions (1.42),(1.44) (1.45) and (1.46)-(1.48). Predictions

for laminates with cracks in 90-layer only are validated comparing with results from direct FEM calculations and further, see Section 1.5.2, verified comparing with experimental data obtained in our laboratory or found in literature. Comparison is made for different types of glass fiber/epoxy and carbon fiber/epoxy systems and different laminate lay-ups.

COD dependent thermo-elastic properties

The five materials used in COD dependent properties simulations are defined in Table 1.3.

Table 1.3. *Material properties for materials used for calculations and validation.*

Materials	$\mathbf{E_1}$ (GPa)	$\mathbf{E_2}$ (GPa)	$\mathbf{G_{12}}$ (GPa)	$\mathbf{\upsilon_{12}}$	$\mathbf{\alpha_1}$ (10^{-6} 1/ºC)	$\mathbf{\alpha_2}$ (10^{-6} 1/ºC)	**Lamina thickness** (mm)
GF/EP[1]	46.50	22.82	8.60	0.30	10.00	20.00	0.150
GF/EP[2]	41.70	13.00	3.40	0.30	-	-	0.150
GF/EP[3]	44.73	12.76	3.50	0.30	-	-	0.138
GF/EP[4]	44.73	12.76	3.50	0.30	-	-	0.148
CF/EP	138.00	10.30	5.50	0.30	0.43	25.87	0.125

First laminates with one crack system only were considered. The goal was a) to validate the developed general expressions for calculation of all thermo-elastic constants of the damaged laminate and b) to study the crack interaction effects in order to establish the crack density region where the concept of non-interactive cracks and the obtained power law can be used. Predictions of properties degradation were compared with direct FEM results. Considering cross-ply laminate with cracks in 90-layer only the axial modulus E_x, Poisson's ratio ν_{xy} and the thermal expansion coefficient α_x were calculated using Equations (1.31) - (1.41). The general expressions (1.25) and (1.29), (1.30) were also used and the results were as expected identical. Predictions of the axial modulus, Poisson's ratio and thermal expansion coefficient are presented in a normalized form for [0,90]s GF/EP[1] laminate in Fig. 1.9. Results of direct FE calculations in

generalized plane strain formulations are also presented there. Obviously model predictions have very high accuracy in non-interactive crack density region. Since the high accuracy of the power law for COD was already established this proves the validity of the used relationships between global material response and local field parameters. With increasing crack density deviations can be noticed: model, which uses COD's of non-interactive cracks, predicts too large change of thermo-elastic properties. Noticeable deviations for the considered laminate start at crack density larger than 1.5 cr/mm. Attempt to improve predictions using the crack interaction function for system of cracks in an infinite medium suggested by Gudmundson et al.,(1993) failed: the interaction using his model is significantly overestimated.

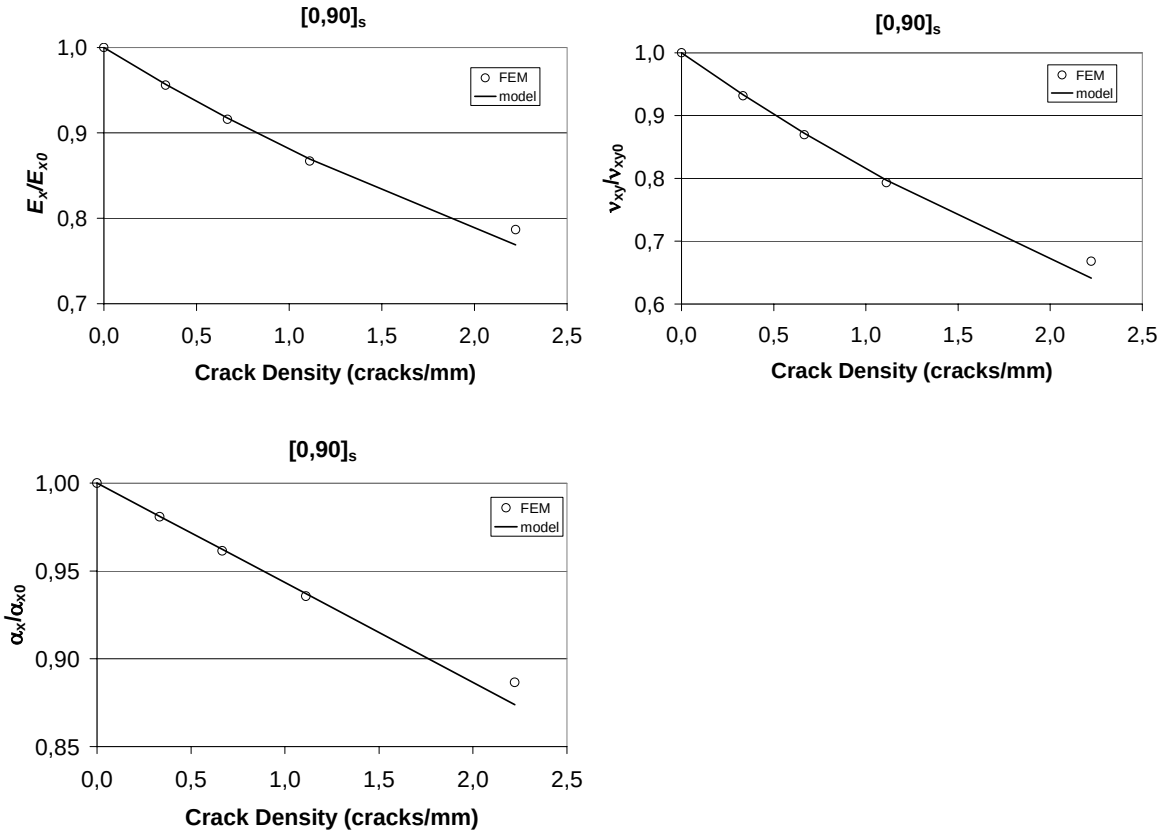

Figure 1.9. *Thermo-elastic properties degradation in GF/EP[1] $[0,90]_s$ cross-ply laminate due to cracks in 90- layer.*

Secondly, cross-ply laminates with two orthogonal systems of cracks were investigated, see Fig. 1.1.

Since no elastic modulus data for laminates with two orthogonal systems of cracks are available, comparison in this case is made with Hashin's model and with 3-D FEM calculations with a very fine mesh. The same crack density $2l_{90}/t_{90} = l_0/t_0 = 5$ corresponding to non-interactive case was used in both layers. The stiffness of [0,90]s cross-ply laminate with cracks in both 90 and 0-layer was calculated with the same number of elements in x,z- and y,z-plane. The total number of elements used was 36000 and for one particular case even 80000. In other words the number of elements in the mesh was varied to find the most suitable mesh, taking both the calculation time and accuracy into consideration.

Here one of the goals was to investigate the interaction effects between cracks belonging to different crack systems. This is of importance because equations in Section 1.2 are valid also for interactive cracks but the power law for COD is established neglecting any interaction. From the analysis presented above we know the interaction distance between cracks belonging to the same crack system.
Considering the interaction between a crack in 90-layer and a crack in 0-layer we can expect that crack in, for example, 0-layer will slightly reduce the average stiffness of this layer. According to performed COD analysis this will result in a slightly higher opening of the crack in the other layer, which implies that the stiffness using a very fine 3-D mesh should be slightly lower than the predicted by power law.

The reduction in elastic properties for laminates with cracks in both layers is summarized in Table 1.4. At first the difference between results is about 0.1% for E-moduli and thermal expansion coefficients and about 2% for Poisson's ratios. The second observation is that a very fine mesh leads to systematically slightly lower values than using analytical model. That may indicate an interaction effect between these two orthogonal cracks but may also be due to the mesh refinement or the approximate nature of the power law. Since the difference is small we conclude that the interaction effects between cracks in 90-layer and 0-layer may be neglected. Using mesh with 80000 elements led to further decrease of normalized E-modulus from 0.9151 to 0.9144.

***Table 1.4**. Comparison between FEM and the present model for GF/EP[1] $[0,90]_s$ cross-ply laminate with cracks in both 0- and 90- layer.*

	FEM	**model**
E_x/E_{x0}	0.9151	0.9162
E_y/E_{y0}	0.9076	0.9072
ν_{xy}/ν_{xy0}	0.7982	0.8195
ν_{yx}/ν_{yx0}	0.7935	0.8114
α_x/α_{x0}	0.9557	0.9576
α_y/α_{y0}	0.9521	0.9534

Comparison between the developed model and Hashin's variational model (Hashin, 1987) based on results for GF/EP[2] [0,90]s laminate with the same number of cracks in both layers is presented in Figure 1.10.

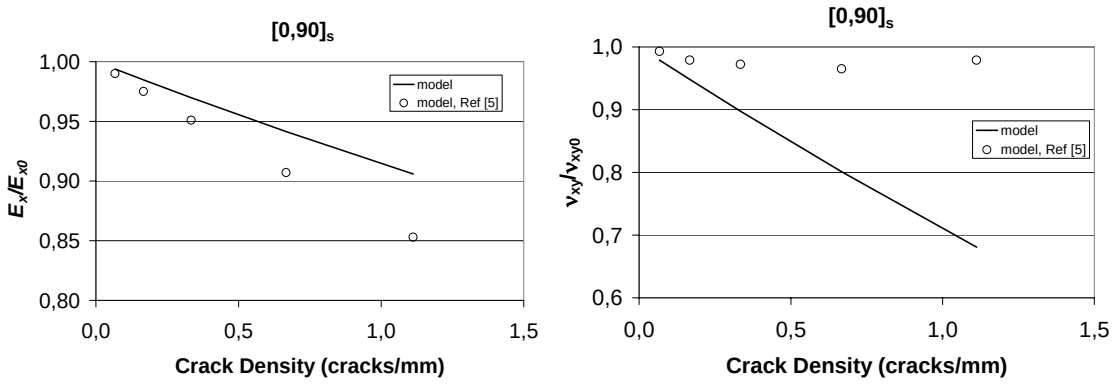

***Figure 1.10.** Elastic properties degradation in GF/EP[2] $[0,90]_s$ cross-ply laminate due to cracks in 0- and 90- layer.*

The Young's modulus reduction predicted by Hashin's model is significantly lower than according to our model which we believe is more accurate. The too low modulus predicted by Hashin's model is a consequence of the used very simple stress

approximations in combination with the principle of complementary energy which gives lower bound to the exact solution. Hashin's predicted Poisson's ratio is incorrect because of his erroneous definition of the average transverse strain in corresponding expression for Poisson's ratio.

CSD related properties

The shear modulus simulations reported below are divided into two sections. The first considers cracks in only one layer (inside or outside) whereas the second one deals with two orthogonal systems of cracks. Equation (1.25) easily deals with cracks in several layers at the same time but the COD's and the CSD's must be modified. They can still be calculated using the power law expressions but the constraint layer effective stiffness must be reduced to account for the damage in the constraint layer. An iterative procedure has been used to calculate the interaction of cracks belonging to different layers.

Simulating shear modulus reduction in laminate with **one system of cracks** the power law equation (46) with the obtained parameters (1.47) and (1.48) was used in equation (40) to predict the shear modulus of a $[S_m,90_n]_s$ and $[90_n,S_m]_s$ laminates with transverse cracks in 90-layer. The notation S_n was explained earlier. In Fig. 1.11, the modulus predictions from the model are compared with direct FE-calculations for inside cracks. In Fig. 1.11a the shear modulus ratio $G_{12}/G_{xy}^{s}=1$ and in Fig. 1.11b $G_{12}/G_{xy}^{s}=0.5$. Fig. 1.12 shows the accuracy of the model for outside cracks, $G_{12}/G_{xy}^{s}=1$.

The reduction in shear modulus due to transverse cracks is predicted with a high accuracy. The reduction is higher in Fig. 1.11a due to lower shear modulus (smaller constraining effect) from the undamaged layer.

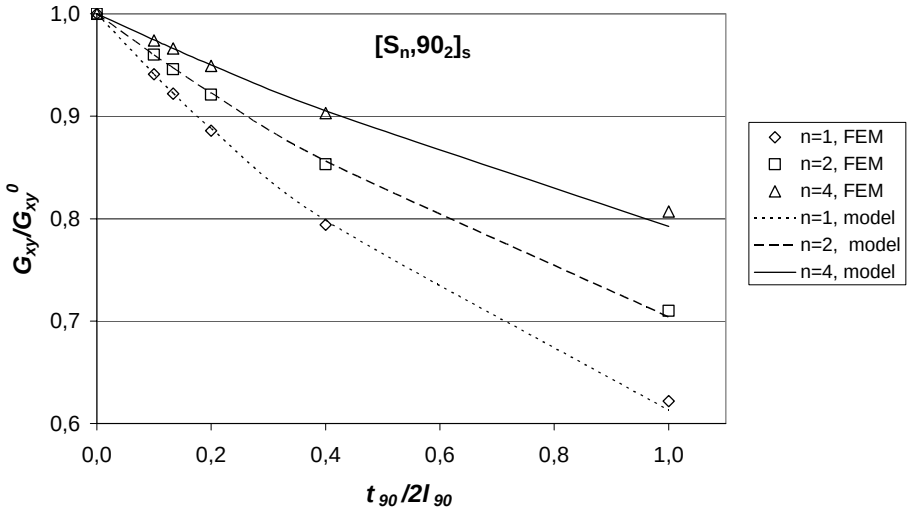

Figure 1.11a. *Reduction in shear modulus due to transverse cracks in 90-layer from direct FE-calculations and model for GF/EP, $G_{12}/G_{xy}^{s}=1$.*

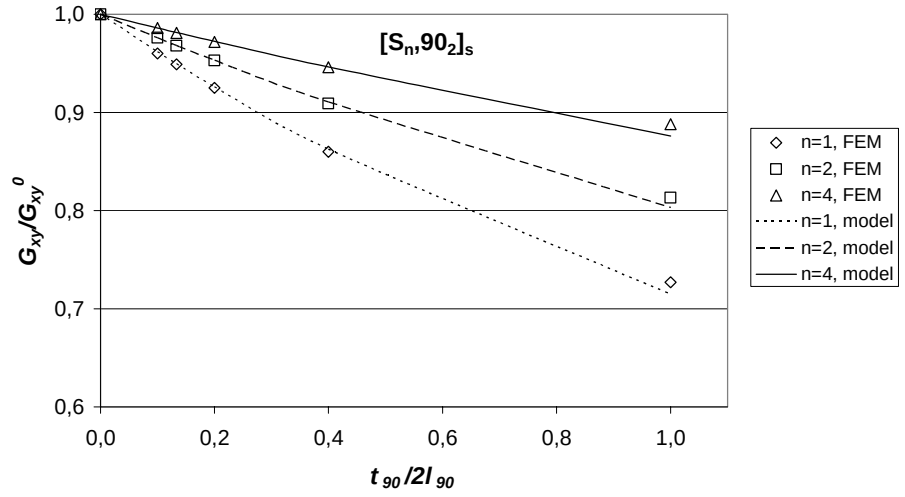

Figure 1.11b. *Reduction in shear modulus due to transverse cracks in 90-layer from direct FEM-calculations and model for GF/EP, $G_{12}/G_{xy}^{s}=0.5$.*

The model prediction for low crack densities is excellent but for large crack densities a small deviation is observed. This is probably because the cracks start to interact.

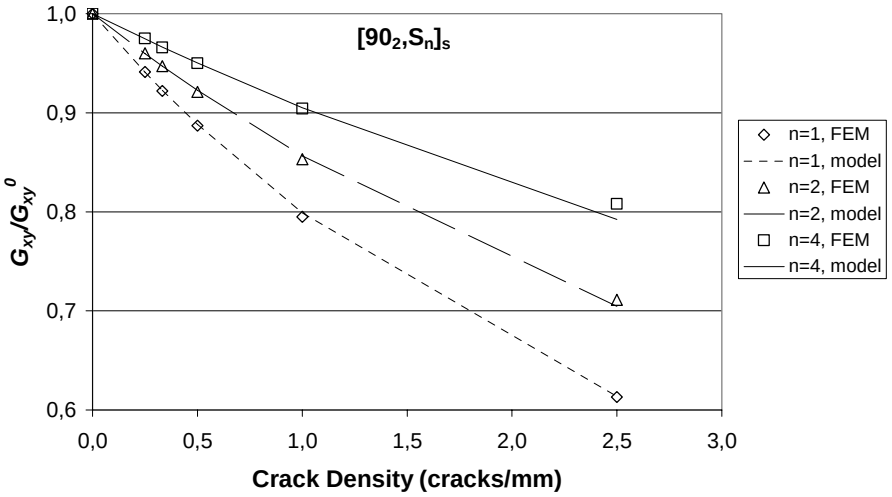

Figure 1.12. *Reduction in shear modulus due to transverse cracks in 90-layer from direct FE-calculations and model for GF/EP,* $G_{12}/G_{xy}^{s}=1$.

In Fig. 1.13 the FE-model is compared with Tao's and Sun's (1993) FE-calculations for $[0_2,90]_s$ CF/EP[1] . The agreement is excellent. Their results are taken from a plot which makes it difficult to find the values with a high accuracy, but they are accurate enough to prove that our FE-model predicts the same shear modulus as their. Fig. 1.13 is a validation that the power law is applicable also for CF/EP systems.
The model is compared with Hashin's model (1985) in Figure 1.14. The result is as expected; his model gives a lower bound of the solution and therefore overestimates the shear modulus reduction of the laminate.

The shear response of cross-ply laminates with **cracks in both 0- and 90-layers** has been previously analyzed in the framework of a shear lag model in Tsai et al.(1990), Henaff-Gardin (1996), Kashtalyan et al. (2000). It was shown by Kashtalyan et al., (2000) that the "superposition of solutions" suggested in Tsai et al. (1990) leads to large errors.

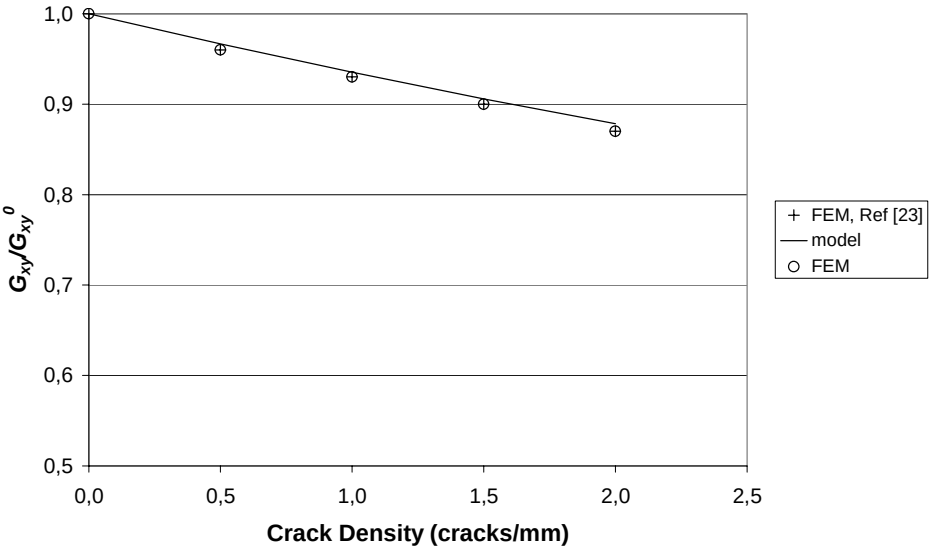

Figure 1.13. *Model predictions and FE-calculations compared with Sun and Tao's FE-calculation for CF/EP-1 $[0_2,90]_s$ laminate.*

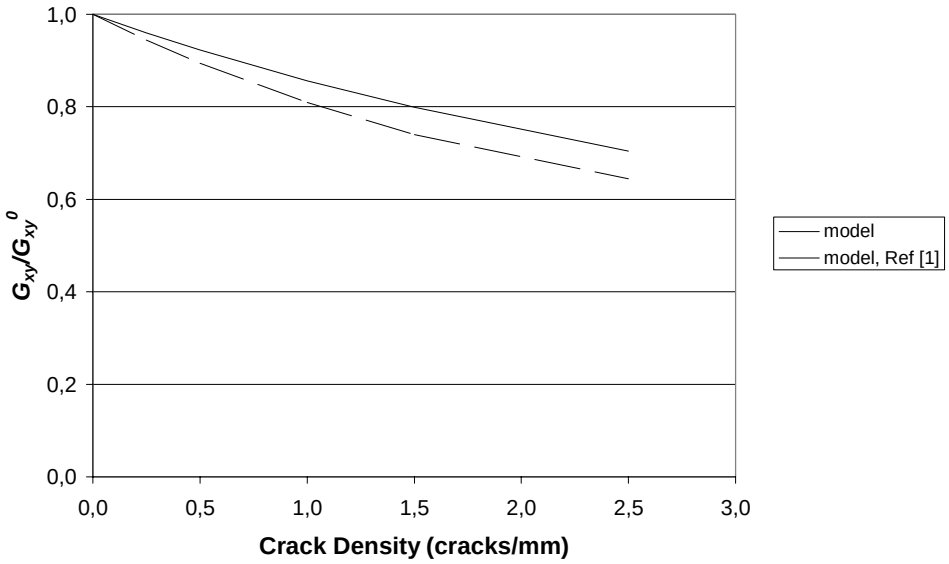

Figure 1.14. *Comparing model prediction with Hashin's model for GF/EP $[0_2,90_2]_s$ laminate.*

Superposition means that the shear modulus reduction due to 90-cracks only is added to the laminate shear modulus reduction due to 0-cracks only. Since Lundmark et al. (2005) demonstrated using FEM that this approach is very accurate when considering Young's moduli and Poisson's ratios of the cross-ply laminate, this question deserves a special discussion. The COD of cracks in the 90-layer which governs the elastic modulus reduction depends on the axial stiffness ratio of both layers. However, the effect of cracks in the 0-layer on the effective axial stiffness of the 0-layer is negligible. In contrary cracks in the 0-layer have a very large effect on the effective shear stiffness of this layer which governs the CSD of the crack in the 90-layer. In result the CSD is larger if the presence of cracks in the constraint layer is accounted for.

Therefore, calculating the crack face sliding displacement CSD according to the power law (46) the effective shear modulus of the neighbouring layer has to be used if these layers have cracks. It can be achieved using an iterative procedure.

In first iteration the interactive CSD's of a 0-layer crack and a 90-layer crack in a $[0_n,90_m]_s$ laminate may be obtained following the procedure described below. The index in parenthesis denotes the current iteration.

a) Crack face sliding displacement of the crack in the 0-layer, CSD-0(1).

In order to calculate CSD-0(1) we first have to determine the effective shear modulus of the neighbouring 90-layer with cracks. Therefore we consider a crack in the 90-layer and calculate, using the power law given by equations (1.46) - (1.48), the CSD of the 90-layer crack assuming that the effective shear modulus of the 0-layer $G_{eff}^{0^\circ}$ equals to the initial shear modulus of the 0-layer, $G_{eff}^{0^\circ}(0) = G^{0^\circ}$. Since the calculated value, which we are denoting CSD-90(0), is obtained **without** accounting for cracks in the sublaminate it is a zero approximation. We can use CSD-90(0) to calculate using equation (1.40) the shear modulus $G^{LAM}(1)$ of the $[0_n,90_m]_s$ laminate with cracks in 90-layer only. Now the effective shear modulus of the damaged 90-layer can be back-calculated using the CLT.

$$G_{eff}^{90^\circ}(1) = \frac{(t_0 + t_{90}/2)\,G^{LAM}(1) - t_0 G_{eff}^{0^\circ}(0)}{t_{90}/2} \tag{1.49}$$

Finally the CSD of the 0-layer crack, CSD-0(1) can be calculated applying equations (1.46) - (1.48) and using $G_{eff}^{90^\circ}(1)$ as the effective shear modulus of the 90-layer.

b) Crack face sliding displacement of the crack in the 90-layer, CSD-90(1).

This time in order to use equations (1.46) - (1.48) we need the effective shear modulus of the neighbouring 0-layer with cracks. Therefore we first consider a crack in the 0-layer and calculate, using the power law given by equations (1.46) - (1.48), the CSD of the 0-layer crack assuming that the effective shear modulus of the 90-layer $G_{eff}^{90^\circ}$ equals to the initial shear modulus of the 90-layer, $G_{eff}^{90^\circ}(0) = G^{90^\circ}$. Thus the calculated value CSD-0(0) is obtained **without** accounting for the cracks in the 90-layer. We can use CSD-0(0) to calculate using equation (1.40) the shear modulus $G^{LAM}(1)$ of the $[0_n,90_m]_s$ laminate with cracks in the 0-layer only. Now the effective shear modulus of the damaged 0-layer can be back-calculated using the CLT.

$$G_{eff}^{0^\circ}(1) = \frac{(t_0 + t_{90}/2)\,G^{LAM}(1) - t_{90}/2\,G_{eff}^{90^\circ}(0)}{t_0} \qquad (1.50)$$

Finally the CSD of the 90-layer crack, CSD-90(1) can be calculated applying equations (1.46) - (1.48) and using $G^{0^\circ}(1)$ as the effective shear modulus of the 90-layer.

This procedure can be repeated infinite number of times and hopefully it is converging to some asymptotic value. In Figure 1.15, the CSD for both inside and outside cracks is presented as a function of crack density (same crack density in both layers). The assumption that both crack systems are non-interacting gives horizontal lines, i.e. CSD of a crack is independent of crack density. If the iterative procedure is used, the crack face sliding increases with an increased damage level in the neighbouring layer. The result is shown after the first and the second iteration and may be compared with FE-calculations for 2.5 cracks/mm. It can be seen that after two iterations the CSD does not reach the values from the FE-calculations. The difference between the first and the second iteration is small in comparison with difference between the non-interacting assumption and the first iteration step.

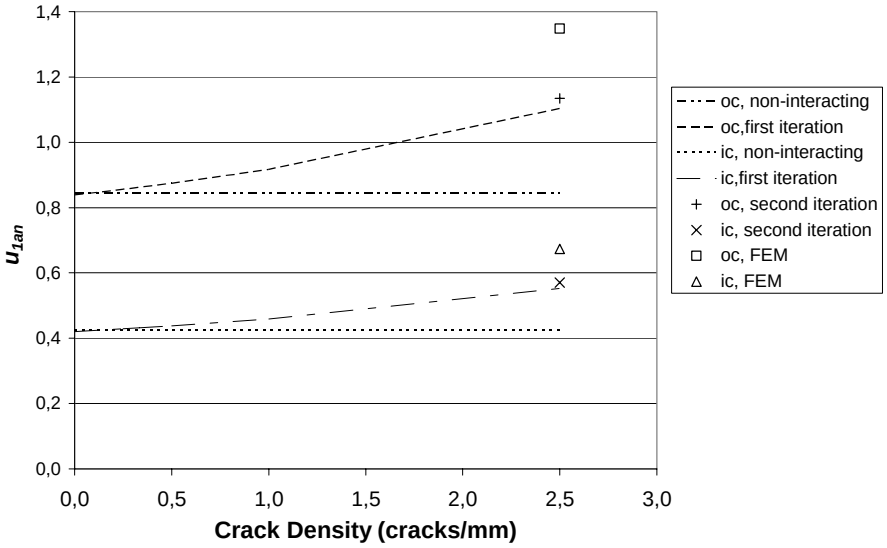

Figure 1.15. *Sliding displacements for both inside cracks (ic) and outside cracks (oc) in a GF/EP $[0_2,90_2]_s$ laminate. Iterative procedure compared with FE-calculations and non-interacting assumption.*

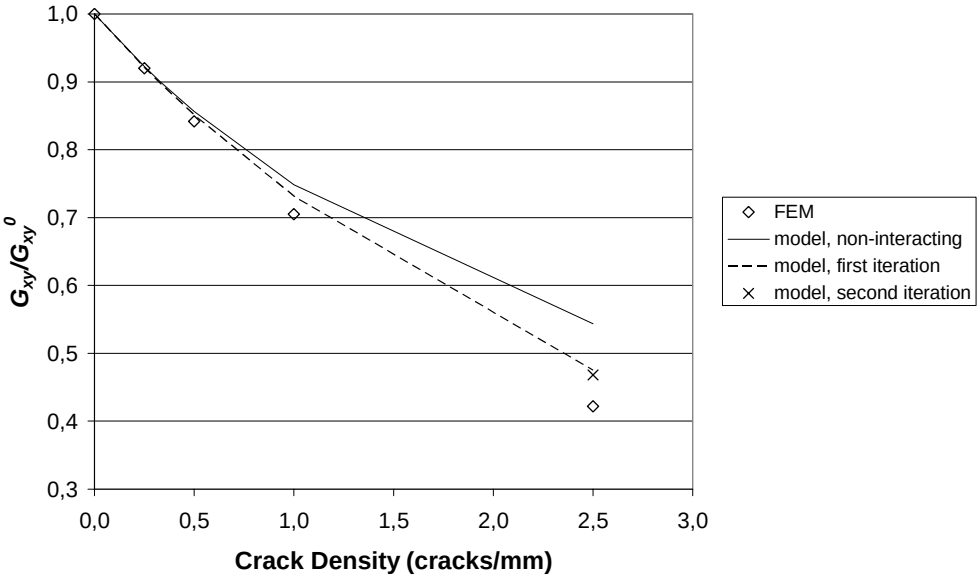

Figure 1.16*. Predictions of the reduction in shear modulus for two systems of cracks in GF/EP $[0_2,90_2]_s$ laminate.*

In Fig. 1.16 the shear modulus predictions are compared with FE-calculations for cracks in both 90 and 0-layer. The crack density is the same in both layers. Fig. 1.16 shows that the model underestimates the effect of crack interaction on the reduction in laminate

shear modulus and it is due to the difference in sliding from FEM and model shown in Fig. 1.15. The source of this difference is unclear at present. May be at high crack density the effective shear modulus of the cracked layer in the power law is not a good descriptor of the interaction between two systems of cracks.

1.5.2 Validation of the Model using Experimental Data

The developed analytical tool is also compared with experimental data for different lay-ups and materials. Considering stiffness of laminates with cracks in 90-layer only, shown in Fig. 1.17 to 1.19, we see that the predictions are in good agreement with test data. Observed deviations may serve for more detailed analysis of the model and of the features of the phenomena. For example, in Fig. 1.17 the reduction of modulus and Poisson's ratio of the damaged $[0_2,90_2]_s$ laminate at large crack densities is slowing down as compared with the model which is a clear indication of the interaction between cracks.

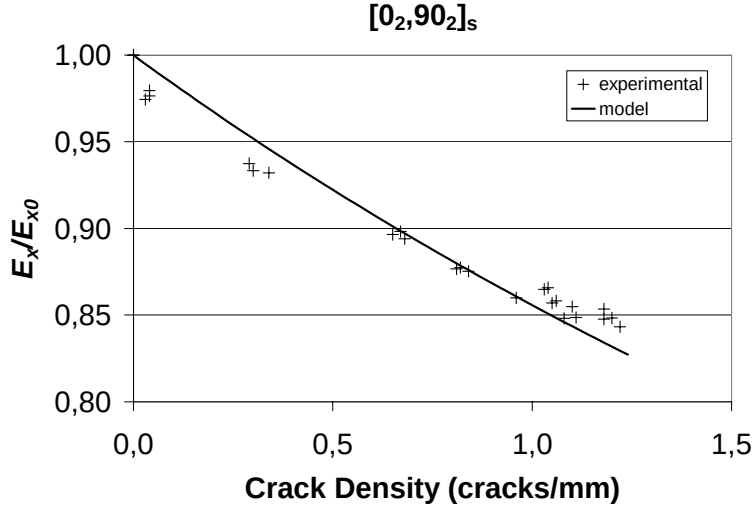

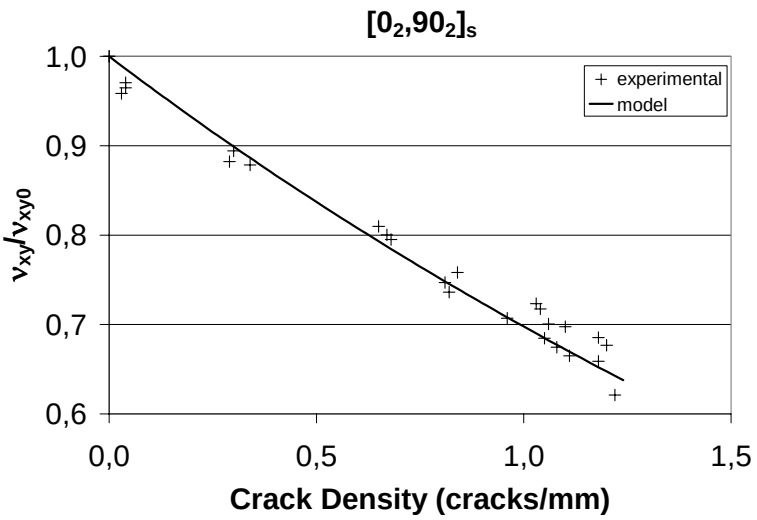

Figure 1.17. *Reduction in elastic properties for GF/EP[3] $[0_2,90_2]_s$ cross-ply laminate. Experimental data compared with model predictions.*

Similar plots for $[0,90_2]_s$ laminate in Fig. 1.18 show the opposite trend: at high crack density the experimental values start to go down faster. We explain this trend by local delaminations at the tip of transverse cracks which start at high loads and which is more pronounced in laminates with large ratio of damaged and supporting layer thickness. So the different layer thickness ratio makes the difference between laminates in Fig. 1.17 and 1.18.

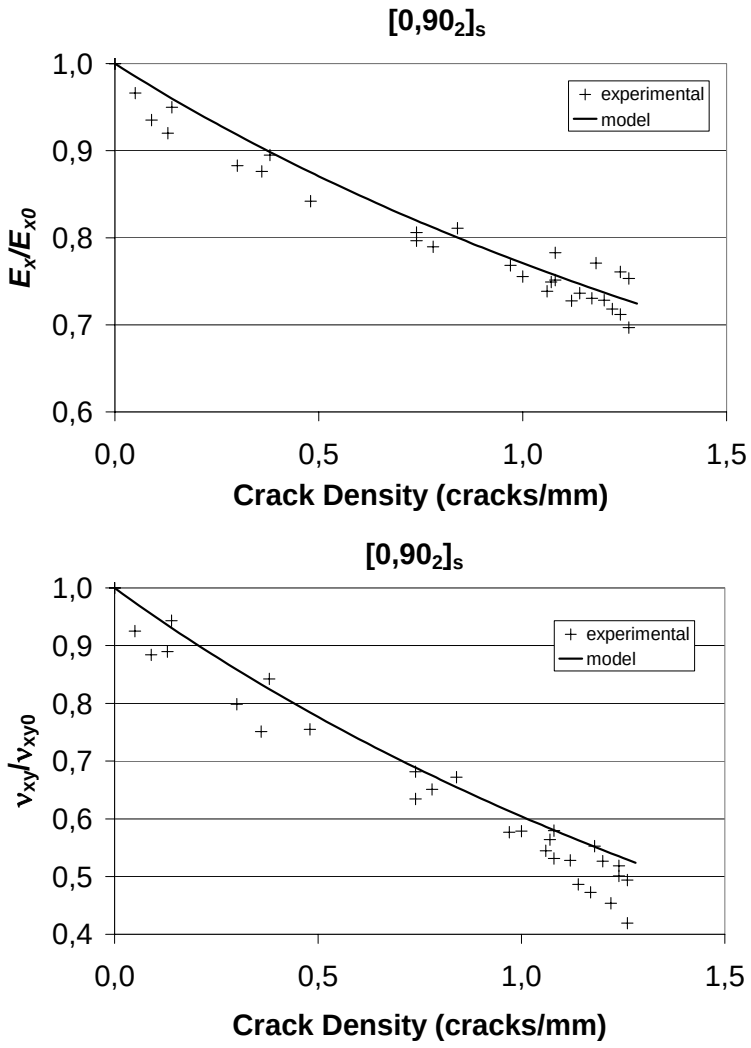

Figure 1.18. *Reduction in elastic properties for GF/EP[3] $[0,90_2]_s$ cross-ply laminate. Experimental data compared with model predictions.*

The model also seems to predict the stiffness reduction for off-axis sublaminate in a good agreement with experimental data, see Fig. 1.19.

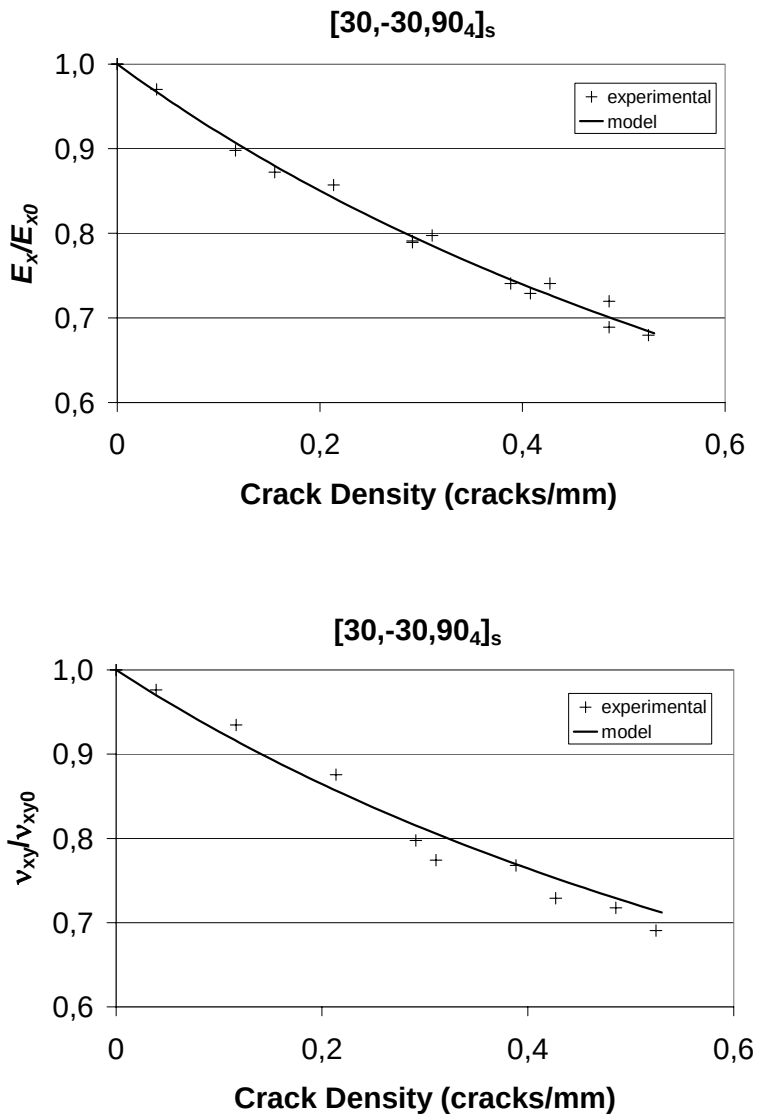

Figure 1.19. *Reduction in elastic properties for GF/EP[4] [30,-30,90$_4$]$_s$ laminate. Experimental data compared with model predictions.*

Next the thermal expansion coefficients were compared with data and predictions given in (Kim et al., 2000). For CF/EP cross-ply laminates with one system of cracks, Fig. 1.20, our predictions are in a very good agreement with experimental data and coincide for low crack densities with predictions based on model in Schoeppner et al., (1998). At large crack densities the difference between predictions increases. However, even if conceptually incorrect for high crack density, our non-interactive COD based predictions

are approximately as good compared to test data as the results of the interactive model Schoeppner et al., (1998). Data and predictions according to both compared models for double-cracked cross-ply laminate are presented in Table 1.3. Even in this case our predictions are rather good and closer to experimental data than model by Schoeppner et al., (1998).

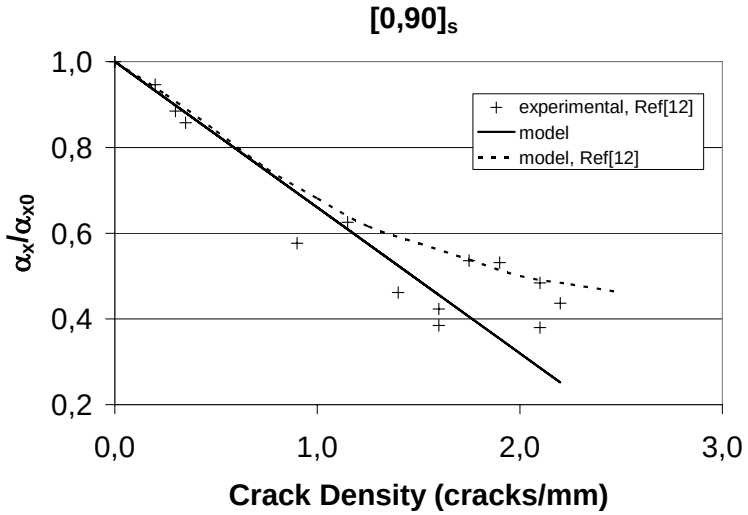

Figure 1.20. *Reduction in thermal expansion coefficient for CF/EP $[0_2,90_2]_s$ cross- ply laminate. Model compared with model and experiment from (Kim et al., 2000).*

Table 1.5*. Reduction in thermal expansion coefficients for CF/EP $[0_2,90_2]_s$ cross- ply laminate with cracks in both 0- and 90-layer.*

ρ_{90}	ρ_0	α_x/α_{x0}	α_x/α_{x0}	α_x/α_{x0}	α_y/α_{y0}	α_y/α_{y0}	α_y/α_{y0}
cracks/m	cracks/m	model	Ref [12] model	Ref [12] exp	model	Ref [12] model	Ref [12] exp
670	390	0.73	0.64	0.72	0.79	0.69	0.78
940	670	0.61	0.56	0.58	0.65	0.60	0.74

Shear modulus of a damaged laminate is analyzed in Fig. 1.21 where the model predictions are compared with predictions and experimental data for inside cracks from Tsai's and Daniel's experiment (1992). Their expression for shear modulus reduction coincides with Hashin's expression and the agreement between the model and

experimental data is excellent. Since we know from Fig. 1.14 that the predictions of the Hashin's model are too low it is not surprising that our predictions which are also presented in Fig. 1.21 show smaller shear modulus reduction. In result we have to question also the accuracy of the experimental data in Tsai and Daniel et al., (1992). Obviously it is very difficult to perform a shear testing of damaged laminates and therefore any attempt is highly appreciated. The problem may be with the data reduction in Tsai and Daniel et al., (1992). The damaged tensile cross-ply specimen which is loaded in in-plane shear (one cross-section is fixed and to another-one is applied a constant tangential in-plane displacement) was described as a Timoshenko beam, which is rather questionable for the length/width ratio used in the test set-up. Another possible source of inaccuracy of the data reduction is that the axial modulus of the damaged laminate, which is also required in the data reduction expressions, is calculated using a shear lag-model.

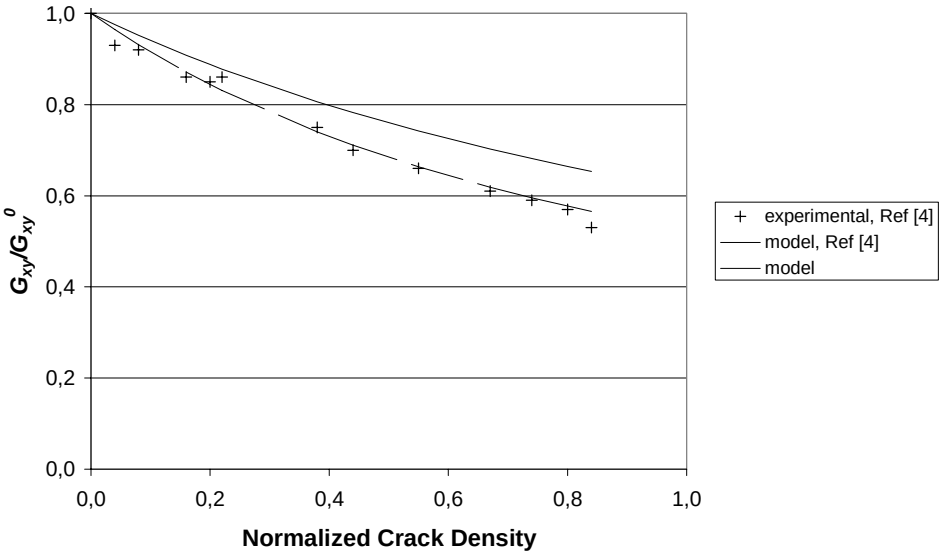

Figure 1.21. *Model predictions compared with experimental data and model for inside cracks from Daniel and Tsai for CF/EP-2 $[0,90_2]_s$ laminate.*

1.6 Range of validity of the analytical approach

The presented model is developed in the framework of elasticity. The well known shear nonlinearity of UD composite, which mainly is caused by visoelastic and viscoplastic

effects, certainly affects the nonlinear stress-strain response of the laminate at high stresses. Therefore, it has to be emphasized that the presented expressions (1.25), (1.29), (1.30) describe the residual stiffness of the damaged composite measured at small strains after viscoelastic relaxation. In other words, laminate may be damaged at high applied load with all nonlinearity effects present, but the stiffness measurements are in a different test performed in the "linearity region".

Realizing the importance of crack face sliding in stiffness reduction, the effect of friction becomes an issue. Friction would reduce the CSD and would lead to smaller stiffness reduction. However, it has to be noted that the term "sliding" is used to describe the tangential component of the displacement together with COD which is the normal displacement. Since in most of laminates, excluding cross-ply in shear, COD is also present, sliding does not imply that the crack faces are in contact. It depends on the sign of the transverse to the crack component of the stress in the layer. The situation becomes even more complex if the damaged laminate is subjected to varying multiaxial loading: frictional contact boundary conditions may change to open crack conditions questioning the meaning of the term "residual stiffness". More experimental evidence is required before deep studies of these effects are started. However, it is always possible to estimate the upper bound of the effect of friction on the residual stiffness by performing two calculations for a multidirectional laminate: a) allowing free sliding and opening; b) allowing only opening and assuming zero sliding.

Local inter-layer delaminations often develop at the tip of intralaminar cracks. They can be easy included in the presented stiffness calculation model through the value of the COD and CSD which is larger for cracks with delaminations. Parametric analysis would lead to new expressions for COD's and CSD's which would include also the size of the delamination. However, preliminary results show that small local delaminations (of size of 1-2 fiber diameters) have a negligible effect on the COD. If delaminations – interface cracks are not connected to intralaminar cracks their effect on diagonal elements of the extensional stiffness matrix of the laminate may be neglected because the main effect will be on the bending stiffness. The effect on laminate shear modulus may be predicted using the framework used here. The dependence of the interface crack face displacements on geometrical and elastic parameters has to be investigated numerically.

1.7 Conclusions for Chapter 1

The stiffness matrix and thermal expansion coefficients of a laminate with intralaminar cracks in layers may be predicted with confidence using the exact expressions obtained in this paper. Relationships, expressing the laminate thermo-elastic properties dependence on density of cracks in layers in a matrix form, depend on thermo-elastic properties of layers, geometrical parameters characterizing laminate architecture and the normalized Crack opening displacement (COD) and crack face sliding displacement (CSD).

The normalized COD and CSD are load independent and depend only on the constraint of the surrounding layers. Analysis of non-interactive cracks by FEM showed that COD and CSD are robust parameters which have a power law dependence on layer stiffness (axial and in-plane shear moduli) and thickness ratio.

The thermo-elastic properties predictions based on the developed analytical method are in excellent agreement with direct 2-D FEM calculations for cross-ply laminates with one system of cracks. The interaction between cracks of the same system is significant at large cracks densities and must be included in the approximate expressions for normalized displacements.

The applicability of the power laws, obtained analyzing non-interactive cracks (only one system of cracks present and the distance between cracks is large), in problems with several crack systems and large crack density was inspected comparing predictions with direct 3-D FEM calculations. 3-D FEM calculations for cross-ply laminates with two orthogonal crack systems showed that the interaction between cracks belonging to layers with different orientation is negligible when the laminate axial modulus is calculated whereas it is significant calculating the laminate shear modulus.

The model is also in a good agreement with experimental data. However, agreement at large crack densities could be improved, introducing a function accounting for crack interaction. To be able to predict the reduced elastic properties for a more complex laminate, the crack face sliding displacement has to be analyzed, which is left for a separate paper.

2. Modeling UD composite stiffness reduction due to multiple fiber breaks and interface debonding

2.1 Introduction

Multiple fiber fractures are observed in unidirectional (UD) long fiber composites loaded in fiber direction. The number of fiber cracks grows with increasing load and each individual fiber crack can be accompanied by fiber/matrix debonding in the proximity of the crack. An alternative is matrix yielding at the interface in this high shear stress region. The fiber fracture is governed by the statistical nature of the fiber strength distribution and the globally and locally (stress concentrations due to breaks in neighboring fibers) increasing stress. The debond growth along the interface in fatigue and/or increasing macroscopic loading conditions is most probably governed by fracture mechanics parameters.

In this chapter the damage evolution modeling is not considered. Realizing the briefly listed reasons for the existing damage state and leaving the simulation of it for a further study the analysis here is focused on determination of the effect of the damage state on elstic properties of the UD composite.

A large number of research papers have been published on description of the stress transfer from matrix into fiber at the fiber break. Analysis have been analytical, see for example, Cox, (1952), McCartney, (1987), Wu et al., (1998) as well as numerical (Xia et al., 2002) with more focus on short fibers or on the description of the single fiber fragmentation test.. These studies are relevant to the topic of this paper because the average stress in a fiber which may be calculated from the stress distribution is directly linked to the elastic modulus of the damaged composite.

In contrast to the papers which deal with stress distribution models, in this paper we develop relationships which link the entire stiffness matrix of the damaged UD composite with two robust parameters from the local solution: average opening displacement (COD) of the fiber break and its sliding displacement (CSD) both normalized with respect to the size and to the far field stress in the fiber.

In order to use these expressions we need to know the dependence of COD, CSD on fiber and matrix properties, fiber content, debond length etc. This information can be obtained from available analytical stress transfer models. However in this paper we extract these dependences from FEM parametric analysis performed on a model consisting of three concentric cylinders: a) broken fiber; b) matrix cylinder around it; c) large effective composite cylinder surrounding them. The observed trends are described by simple fitting functions which with a high accuracy describe COD's of perfectly bonded and partially debonded cracks. The analysis in this paper is limited by opening displacements only and considering cracks as non-interactive which makes the stiffness predictions conservative.

2.2 Stiffness reduction modeling

The stiffness matrix of the UD composite shown in Fig. 2.1 is given by the relationship between stresses, $\{\sigma\}_{RVE}$ applied to the UD composite RVE and the corresponding strain response, $\{\varepsilon\}_{RVE}$.

$$\{\sigma\}_{RVE} = [Q(D)]^{RVE} \{\varepsilon\}_{RVE} \tag{2.1}$$

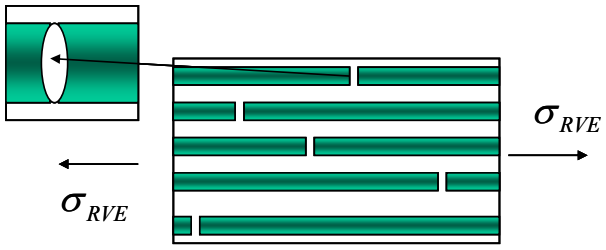

Figure 2.1. *Schematic showing of the UD composite with randomly distributed fiber breaks*

D represents the damage state with fiber breaks which may be accompanied by fiber/matrix interface debonding. Two types of cylindrical elements may be recognized in the Representative Volume Element (RVE) of a UD composite. The first element group is fibers with orientation which coincides with the global axis of the composite RVE. Obviously in the case of a UD composite local and global coordinate systems coincide. The second is matrix regions which also have cylindrical form. Each element is characterized by its volume fraction in the RVE (V_f and V_m), geometry of the element (circular cross-section of the fiber with radius r_f), constituent stiffness matrices $[Q]_f$ and $[Q]_m$ which are defined by a linear elastic constitutive law

$$\{\sigma\}_k = [Q]_k \{\varepsilon\}_k \qquad \text{k=f,m} \tag{2.2}$$

In (2.2) $\{\sigma\}_k$, $\{\varepsilon\}_k$ are strain and stress vectors for the k-th element.

According to (A1.4) and (A1.5) in Appendix 1

$$\{\sigma\}_{RVE} = \sum_k V_k \{\sigma\}_k^a = V_f \{\sigma\}_f^a + V_m \{\sigma\}_m^a \tag{2.3}$$

Using averaged Hook's law (A1.9) in (2.3) we obtain

$$\{\sigma\}_{RVE} = \sum_k V_k [Q]_k \{\varepsilon\}_k^a \tag{2.4}$$

Replacing in (2.4) volume averaged strain (over the element) by boundary averaged and Vakulenko-Kachanov tensor (A1.7) we obtain

$$\{\sigma\}_{RVE} = \sum_k V_k [Q]_k \left(\{\varepsilon\}_k^{ba} + \{\beta\}_k\right) \tag{2.5}$$

Eq. (2.5) may be used to represent cracks in both, fibers and in the matrix. In the present study we will consider only fiber cracks, thus assuming that $\{\beta\}_m = 0$. The effect of the debonded interface at fiber breaks will be represented by increasing displacements of the crack surfaces.

The boundary averaged strain of an element is expressed through its surface displacements, see (A1.6). Hence in elastic problem it is a linear combination of strains applied to the RVE

$$\{\varepsilon\}_k^{ba} = [H]_k \{\varepsilon\}_{RVE} \quad \text{or} \quad \begin{Bmatrix} \varepsilon_L \\ \varepsilon_T \\ \gamma_{LT} \end{Bmatrix}_k^{ba} = \begin{bmatrix} H_{11} & H_{12} & H_{16} \\ H_{21} & H_{22} & H_{26} \\ H_{61} & H_{62} & H_{66} \end{bmatrix} \begin{Bmatrix} \varepsilon_L \\ \varepsilon_T \\ \gamma_{LT} \end{Bmatrix}_{RVE} \tag{2.6}$$

Elements of the H-matrix are very complex functions of element properties, internal geometry of the RVE which may be obtained from numerical solution of the local problem. Generally speaking the H-matrix may change with damage evolving inside of the k-th element, which could be presented as

$$[H]_k = [H]_k^0 + [H]_k^D \tag{2.7}$$

However, in the present study we assume that the second term in (2.7) is relatively small and neglect it. Hence

$$[H]_k = [H]_k^0 \tag{2.8}$$

The $\{\beta\}_f$ vector for the fiber is expressed through crack face displacements which are proportional to the number of fiber breaks N represented by normalized crack density $\rho_n = \frac{N}{L} r_f$, proportional to the far-field stress in the fiber $\{\sigma_0\}_f$ (average fiber stress at the same applied load to the undamaged RVE in the absence of fiber break). Hence, it can be written in the following form

$$\{\beta\}_f = -\frac{\rho_n}{E_{fL}} [U]_f \{\sigma_0\}_f \tag{2.9}$$

The longitudinal fiber modulus E_{fL} is introduced (2.9) to have the crack face displacement matrix $[U]_f$ dimensionless. The "far field" stress $\{\sigma_0\}_f$ can be expressed through the strain applied to RVE of an undamaged composite in the following form

$$\{\sigma_0\}_f = [Q]_f \{\varepsilon_0\}_f^a = [Q]_f \{\varepsilon_0\}_f^{ba} = [Q]_f [H]_f^0 \{\varepsilon\}_{RVE}^0 \tag{2.10}$$

Now

$$\{\beta\}_f = -\frac{\rho_n}{E_{fL}} [U]_f [Q]_f [H]_f^0 \{\varepsilon\}_{RVE}^0 \tag{2.11}$$

Substituting (2.6) and (2.11) in (2.5) we obtain

$$\{\sigma\}_{RVE} = \sum_k V_k [Q]_k [H]_k^0 \{\varepsilon\}_{RVE} - V_f \frac{\rho_n}{E_{fL}} [Q]_f [U]_f [Q]_f [H]_f^0 \{\varepsilon\}_{RVE}^0 \tag{2.12}$$

From (2.12) the stiffness matrix of the undamaged composite is

$$[Q]_0^{RVE} = \sum_k V_k [Q]_k [H]_k^0 \tag{2.13}$$

Since for the applied stress $\{\sigma\}^{RVE}$ the strain response of the undamaged composite will be

$$\{\varepsilon\}_{RVE}^0 = [S]_0^{RVE} \{\sigma\}_{RVE} \tag{2.14}$$

we obtain from (2.12)

$$\{\sigma\}_{RVE} = \left[[I] + V_f \frac{\rho_n}{E_{fL}} [Q]_f [U]_f [Q]_f [H]_f^0 [S]_0^{RVE} \right]^{-1} [Q]_0^{RVE} \{\varepsilon\}_{RVE} \tag{2.15}$$

Obviously the stiffness of the damaged composite is

$$[Q]_{RVE} = \left[[I] + V_f \frac{\rho_n}{E_{fL}} [Q]_f [U]_f [Q]_f [H]_f^0 [S]_0^{RVE} \right]^{-1} [Q]_0^{RVE} \tag{2.16}$$

2. 3 Form of the $[H]_k$ matrix

Obviously, an accurate determination of $[H]_k$ is one of the main difficulties in stiffness prediction of undamaged and damaged UD composites. The $[H]_k$ -matrix is defined in the local axes of an element (fiber and matrix cylinders) and it defines the relationship between k-th element boundary averaged strains and the strains applied to the RVE.

$$\{\varepsilon\}_k^{ba} = [H]_k \{\varepsilon\}_{RVE} \tag{2.17}$$

In UD composite each element has a form of a cylinder (with an axis in the L-direction) extending in this direction over the whole length of the RVE. Due to this feature some conclusions regarding the form of the $[H]_k$ -matrix can be formulated.

If only ε_L^{RVE} is applied to the RVE, the strain in each element in the L-direction is equal to the applied strain. Consequently, the elements $H_{11}^f = H_{11}^m = 1$. Applying to the RVE ε_T^{LAM} only (with zero longitudinal strain and shear strain), the average strain in the L-direction in the element is equal to this strain component applied to the RVE (it is zero). Hence $H_{12}^f = H_{12}^m = 0$.

We assume also that only applied RVE shear strains may cause non-zero boundary averaged shear strains in the element leading to $H_{16} = H_{26} = H_{61} = H_{62} = 0$.

The boundary averaged strain in the T-direction in the cylindrical element at applied ε_T^{LAM} is a function of all parameters. The dependence of H_{22} on geometrical and stiffness parameters comes from solution of a complex 3-D problem. The above qualitative analysis leads to the following form of the H-matrix for fiber and for matrix

$$[H]_f = \begin{bmatrix} 1 & 0 & 0 \\ H_{21}^f & H_{22}^f & 0 \\ 0 & 0 & H_{66}^f \end{bmatrix} \qquad [H]_m = \begin{bmatrix} 1 & 0 & 0 \\ H_{21}^m & H_{22}^m & 0 \\ 0 & 0 & H_{66}^m \end{bmatrix} \tag{2.18}$$

H-matrix constants in fiber and in the resin are not independent. One relationship between them may be obtained using the request of thermodynamics that the RVE stiffness matrix of the undamaged UD composite, see (2.13) has to be symmetric.

Two more relationships come from the rule of mixtures (ROM) which exists between the RVE strains and boundary averaged strains in elements. The longitudinal strain ROM is satisfied automatically due to iso-strain state. The transverse strain ROM leads to two independent conditions. Details and derivation are given in Appendix 2. The formulated three conditions for $H_{22}^f, H_{21}^f, H_{22}^m, H_{21}^m$ are used to express three of them through H_{22}^f.

$$H_{21}^f = \left(H_{22}^f - 1\right)\frac{Q_{12}^f - Q_{12}^m}{Q_{22}^f - Q_{22}^m} \tag{2.19}$$

$$H_{21}^m = -\frac{V_f}{V_m} H_{21}^f \tag{2.20}$$

$$H_{22}^m = \frac{1 - V_f H_{22}^f}{V_m} \qquad H_{66}^m = \frac{1 - V_f H_{66}^f}{V_m} \tag{2.21}$$

As a very rough approximation and mainly to demonstrate the approach we can use constant stress models (CSM) used in material mechanics to determine H_{22}^f. According to the constant stress model

$$\varepsilon_T^{RVE} = V_f \varepsilon_T^f + V_m \varepsilon_T^m \qquad \frac{\varepsilon_T^m}{\varepsilon_T^f} = \frac{E_{fT}}{E_m} \tag{2.22}$$

From here

$$\varepsilon_T^{RVE} = \varepsilon_T^f \left(V_f + V_m \frac{E_{fT}}{E_m} \right) \tag{2.23}$$

and $$H_{22}^{f} = \frac{1}{V_f + V_m \dfrac{E_{fT}}{E_m}} \tag{2.24}$$

Similar assumptions regarding shear stresses lead to

$$H_{66}^{f} = \frac{1}{V_f + V_m \dfrac{G_{fLT}}{G_m}} \tag{2.25}$$

Certainly more accurate estimations may be obtained using Concentric Cylinder Assembly model by Hashin et al., (1964), Hashin, (1983) or numerical solutions

2. 4. Crack face displacement matrix $\left[U\right]_f$

The $\left[U\right]_f$ matrix is defined by (9) and its explicit form can me obtained analyzing $\left\{\beta\right\}_f$ which is according to (A1.8) related to crack face displacements.

In the local coordinate system the normal vector of the fiber crack face has only one component

$$n_1 = \pm 1 \qquad n_2 = n_3 = 0 \tag{2.26}$$

Using definition we obtain

$$\beta_{11} = 2\rho_n \frac{u_{1a}}{r_f} \qquad \beta_{22} = 0 \qquad \beta_{12} = -\rho_n \frac{u_{2a}}{r_f} \tag{2.27}$$

In (2.27) u_{1a} and u_{2a} are average displacements of fiber crack faces in the longitudinal and transverse direction respectively

$$u_{1a} = \frac{2}{r_f^2} \int_0^{r_f} \frac{\Delta u_1(r)}{2} r dr \qquad u_{2a} = \frac{2}{r_f^2} \int_0^{r_f} \frac{\Delta u_2(r)}{2} r dr \tag{2.28}$$

In (2.28) Δu is the displacement gap between two crack faces.

Introducing crack face displacements normalized with respect to the crack radius and the far field average stress in the fiber as

$$u_{1an} = \frac{u_{1a}}{r_f}\frac{E_{fL}}{\sigma^0_{Lf}} \qquad u_{2an} = \frac{u_{2a}}{r_f}\frac{G_{fLT}}{\sigma^0_{LTf}} \tag{2.29}$$

we can rewrite (2.26) as

$$\begin{Bmatrix} \beta_{11} \\ \beta_{22} \\ 2\beta_{12} \end{Bmatrix} = -2\rho_n \begin{Bmatrix} u_{1an}\dfrac{\sigma^0_{Lf}}{E_{fL}} \\ 0 \\ u_{2an}\dfrac{\sigma^0_{LTf}}{G_{fLT}} \end{Bmatrix} = -2\frac{\rho_n}{E_{fL}} \begin{bmatrix} u_{1an} & 0 & 0 \\ 0 & 0 & 0 \\ 0 & 0 & u_{2an}\dfrac{E_{fL}}{G_{fLT}} \end{bmatrix} \begin{Bmatrix} \sigma^0_{Lf} \\ \sigma^0_{Tf} \\ \sigma^0_{LTf} \end{Bmatrix} \tag{2.30}$$

Comparing (2.9) with (2.30) we see that $[U]_f$ which enters stiffness reduction expressions is

$$[U]_f = 2\begin{bmatrix} u_{1an} & 0 & 0 \\ 0 & 0 & 0 \\ 0 & 0 & u_{2an}\dfrac{E_{fL}}{G_{fLT}} \end{bmatrix} \tag{2.31}$$

2.5. Factors affecting the normalized average crack opening displacement (NACOD)

The value of u_{1an} depends on the interface quality. If the fiber is debonded the crack opening may be significantly larger. NACOD depends also on fiber volume fraction, elastic properties etc. Micromechanical models developed to describe stress distribution in fiber fragments in SFF test may be used to evaluate the COD. As an alternative to approximate analytical models in this study we performed FEM calculations in axi-symmetrical formulation to calculate the COD. The opening of the penny-shaped crack in longitudinal tension (applied strain 1%) was analyzed considering three concentric

cylinder model. The broken fiber is surrounded by a cylindrical matrix zone which is its turn embedded in a large cylindrical block of the effective composite, see Fig. 2.2. The surrounding composite cylinder is necessary to describe more adequate the effect of neighboring fibers on the local stress distribution. The effective composite properties were calculated using rule of mixtures and Halpin-Tsai expressions. Thus the fiber break effect on effective composite properties in the outer cylinder was not included assuming that the NACOD is not sensitive to about 10% changes in the properties in this cylinder. This argument was also used to justify the use of simplified elastic properties expressions in this region instead of more accurate models like Hashin's concentric cylinder assembly model (Hashin et al., 1964, Hashin, 1983) .

FEM calculations were performed in ANSYS using an axisymmetric formulation. Element type used is the plane element, PLANE82, which is a 2-D, second order element with relatively high accuracy. A non-uniform mesh consisting of both triangular and rectangular elements was used. To obtain higher accuracy a refined mesh (of triangular elements) was used in the vicinity of the crack tip and at the end of the debonding zone.

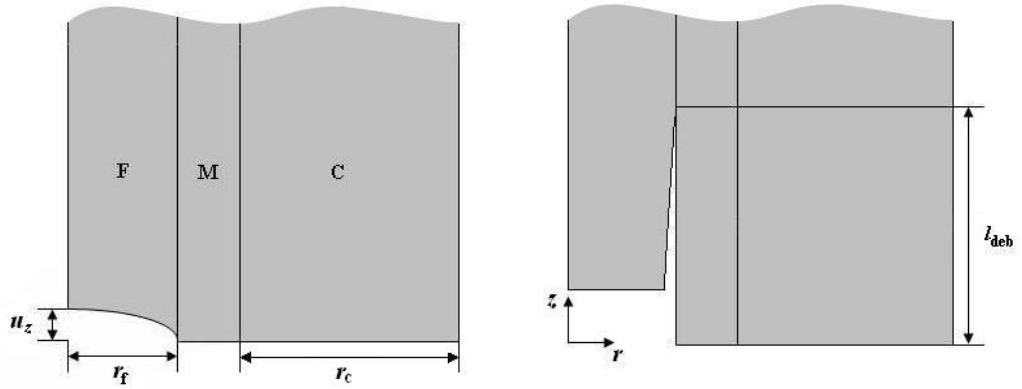

Figure 2.2 *Schematic showing of the model geometry consisting of cylindrical fiber surrounded by matrix cylinder which is embedded in the composite with effective properties: a) perfectly bonded interface; b) partially debonded interface with debond* length l_{deb}

There is a symmetry condition on z = 0, $r \in [0, R]$, where R is the outer radius of the fiber-matrix-composite system. The axisymmetry is around the z-axis. Nodes on the side r = R, $z \in [0, L]$, are coupled in the r-direction. ($L = 90 r_f$ is the length of the fiber-matrix-composite system in the axial direction which represents one half of the distance between two fiber cracks.). The thickness of the effective composite cylinder is $r_c = 5 r_f$. The size of the matrix cylinder depends on the fiber volume fraction V_f. Constant displacement is applied in the z-direction on z= L, $r \in [0, R]$.

The NACOD was analyzed for isolated cracks ($L / r_f = 90$) which are far enough from each other to exclude the stress field interaction effects on the u_{1an}. However, expressions presented above are not limited by the condition of non-interactive cracks. If several cracks in the same fiber would be interacting the NACOD would be smaller. Interaction between cracks in different fibers can also be analyzed but this is out of the scope of this paper and can not be performed using the three cylinder model used here.

Sensitivity analysis was performed to identify some elastic properties of constituents which were expected to have small influence on COD and which could be fixed in the following parametric analyis. Transversally isotropic carbon fiber with 5 elastic constants was used. All (independent) properties are changed with 25%. The elastic modulus E_{fL} affects the COD with about 10% and E_{fT} affects the COD with about 2%. The shear modulus G_{fLT} affects the COD with about 2%. The Poisson's ratios ν_{fLT} and $\nu_{fT\varphi}$ affect the COD with less than 1%. As far as the elastic properties of the matrix concerns, the Poisson's ratio ν_m affects the COD with less than 1%. Although the elastic modulus, E_m, is an independent variable there is no need for a sensitivity analysis because in the parametric analysis all elastic moduli will be normalized with respect to it.

Similar conclusions regarding the significance of Poisson's ratios were obtained for glass fiber composites. It was decided to exclude these parameters from the list of parameters and to assign to them fixed values $\nu_{fLT} = 0.2$, $\nu_{fT\varphi} = 0.45$, $E_m = 3GPa$ $\nu_m = 0.4$

The modulus ratio E_{fL}/E_m and the fiber volume fraction V_f were used as the main parameters in the analysis. A fiber content range $0.45 \le V_f \le 0.55$ which has practical significance was considered.

To account for variability of the radial modulus E_{fT} and shear modulus G_{fLT} the four fiber materials with properties given in Table 2.1 were used.

Table 2.1 *Elastic properties for materials M1 to M4*

Property	M1	M2	M3	M4
E_{fT} (GPa)	20	30	20	30
G_{fLT} (GPa)	30	30	20	20

First the perfect bonding case at the fiber/matrix interface shown in Fig 2.2a) was analyzed. The u^b_{1an} (index b is used to denote the perfectly bonded case) dependence on the fiber/matrix modulus ratio for Material 1 is shown in Fig. 2.3. Obviously, the stiffness ratio has much larger effect on u_{1an} than the variation in fiber volume fraction.

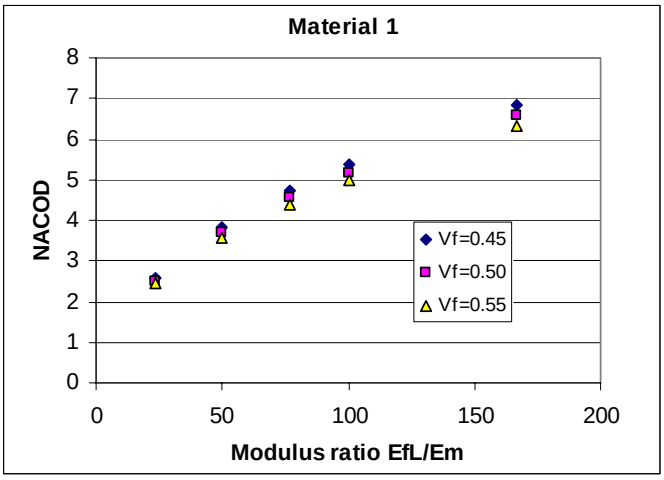

Figure 2.3 *Normalized average COD dependence on fiber/matrix axial modulus ratio.*

Presenting these data in log-log axes as shown in Fig.2.4 we obtain a very straight line with slope which very weakly depends on the fiber content. This result proves that a power law with respect to modulus ratio can give an adequate description of the relationship

$$u_{1an}^{b} = A\left(\frac{E_{fL}}{E_m}\right)^n \tag{2.32}$$

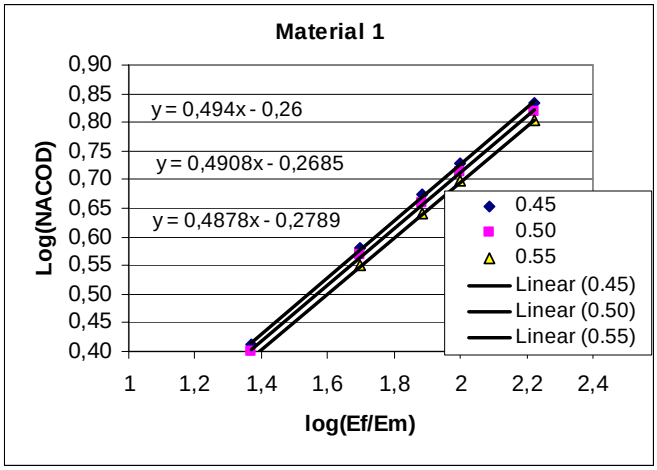

Figure 2.4 *Normalized average COD dependence on fiber/matrix axial modulus ratio in logarithmic axes*

Similar results for Material 2 to 4 show slight dependence of n on the ratio E_{fT}/G_{fLT}. The described dependences are fitted with a high accuracy with the following linear relationship

$$n = 0.5148 + 0.0143\frac{E_{fT}}{G_{fLT}} - 0.066V_f \tag{2.33}$$

A in (2.32) is a function of fiber content V_f and of other elastic properties of the fiber normalized with respect to the matrix modulus

$$E_{fT}^n = E_{fT}/E_m \qquad G_{fLT}^n = G_{fLT}/E_m \tag{2.34}$$

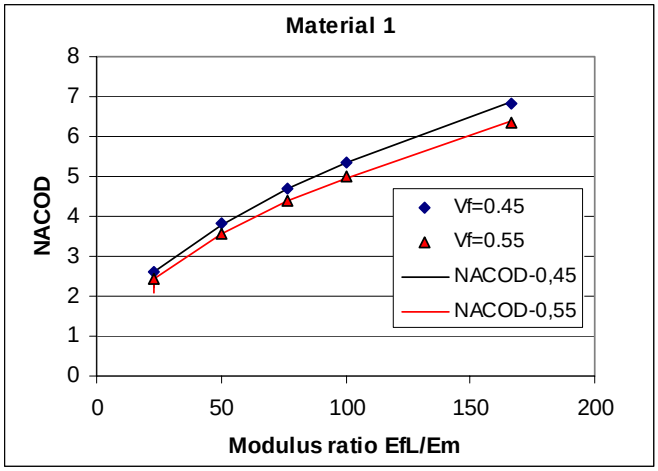

Figure 2.5 *Predicted normalized COD versus calculated using FEM. Predictions are presented by solid lines.*

Analysis of FEM results showed that $\log A$ is a linear function of V_f. The dependence on normalized parameters (2.34) was presented by polynomial expansion

$$-\log A = V_f\left(0.194 - 0.0018E_{fT}^n\right) + a_0 + a_1E_{fT}^n + a_2G_{fLT}^n + a_3E_{fT}^nG_{fLT}^n \qquad (2.35)$$

$$a_0 = 0.0941 \qquad a_1 = 0.00927 \qquad a_2 = 0.00387 \quad a_3 = -0.000234 \qquad (2.36)$$

The predicting accuracy of (2.32)-(2.36) is demonstrated in Fig. 2.5 and 2.6 which shows excellent agreement with FEM values represented by symbols

As a final check of the application range we apply the obtained fitting law to glass fiber composite case ($E_f = 70GPa$, $\nu_f = 0.2$) which due to fiber isotropy is outside the region which was used for fitting parameter determination. In this case, see Fig. 2.7 the predicted normalized average COD's are about 10% lower than the FEM values. This means that the fitting functions are more accurate for anisotropic fibers. However, as it

will be shown in following the interface debonding introduces much larger opening displacements and the obtained 10% underestimation for glass fiber case is acceptable.

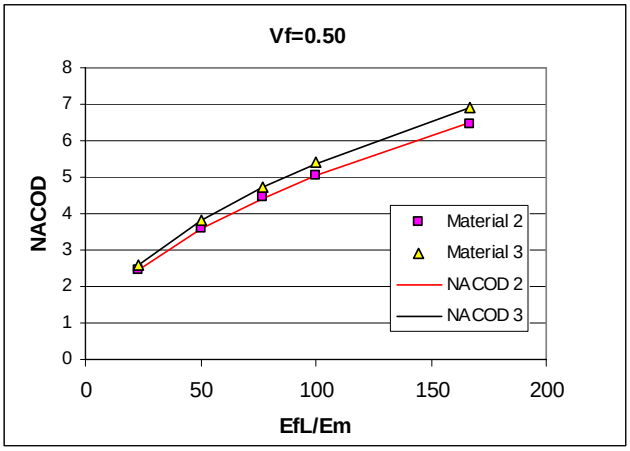

Figure 2.6 *Normalized average COD Predictions according to (2.32)-(2.36) (solid lines) and according to FEM (symbols)*

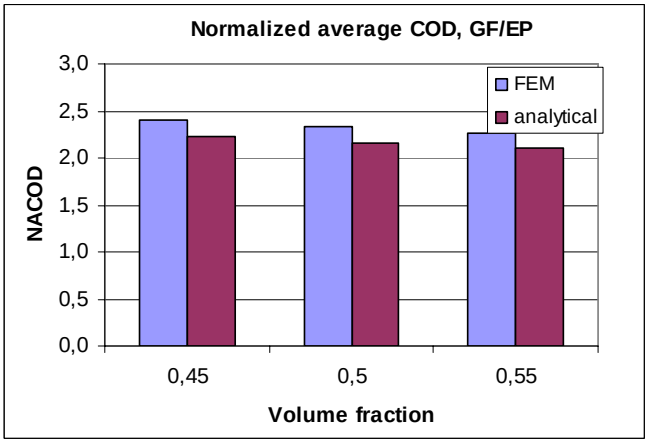

Figure 2.7 *Accuracy of predictions for glass fiber composite*

In most cases the interface at the fiber break is partially debonded and the debond length l_{deb}, see Fig.2.2b), grows with increasing load or with the number of cycles in fatigue. Calculations were performed only for $V_f = 0.45$. The used carbon fiber properties are

$$E_{fL} = 500GPa \qquad E_{fT} = 30GPa \qquad G_{fLT} = 20GPa \tag{2.37}$$

The effect of the debond length l_{deb} on the carbon fiber crack opening profile is shown in Fig.2.8. Obviously the COD significantly increases with the debond length and the coordinate dependence is smaller.

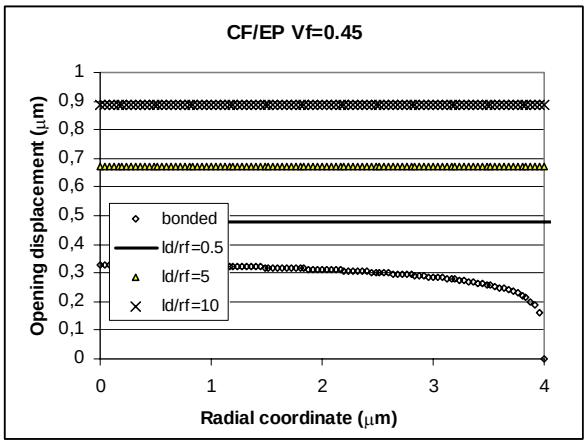

Figure 2.8 *Crack opening displacement profiles at 1% applied strain for different normalized length of debond* l_{deb}. *Friction is ignored.*

Calculations were performed for the following four cases: 1) without contact elements thus allowing for material interpenetration (results in Fig 2.8); 2) with contact elements but with zero friction. The opening profile almost coincides with the case 1); 3) contact elements with friction coefficient $k = 0.2$ (Coulombs friction); 4) contact elements with friction coefficient $k = 0.4$. Calculations were performed without account for thermal effects. Hence, the friction is caused by differences in Poisson's ratios only.

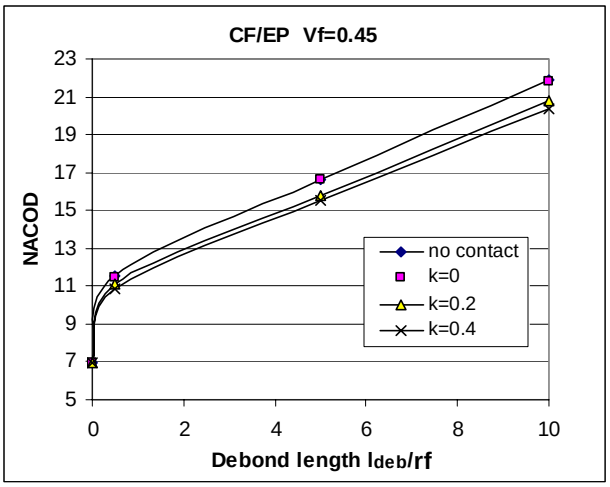

Figure 2.9 *Normalized average COD dependence on the normalized debond length* l_{deb}/r_f *in carbon fiber/ epoxy composite for solution without contact elements and for solution with contact elements and three values of frictional coefficient* k.

The normalized average COD as a function of the debond length is presented in Fig. 2.9 for carbon fiber composite and in Fig. 2.10 for glass fiber composite. The average normalized COD, u_{1an} is a linear function of the debond length for debond length $l_{deb} > 0.5r_f$. Results are almost coinciding for no-contact case and for contact elements with $k = 0$. The presence of friction reduce the slope by 5-10%. The slope is rather insensitive to k change in the region $0.2 \le k \le 0.4$ used in calculations. The slope in the frictional case is very close to one which leads to the following choice of fitting function for COD in this region

$$u_{1an} = 1\frac{l_{deb}}{r_f} + D \qquad (2.38)$$

where D depends on material properties. It is equal to the normalized average COD at $l_{deb} = 0.5r_f$. D is much larger for CF case than for GF case.

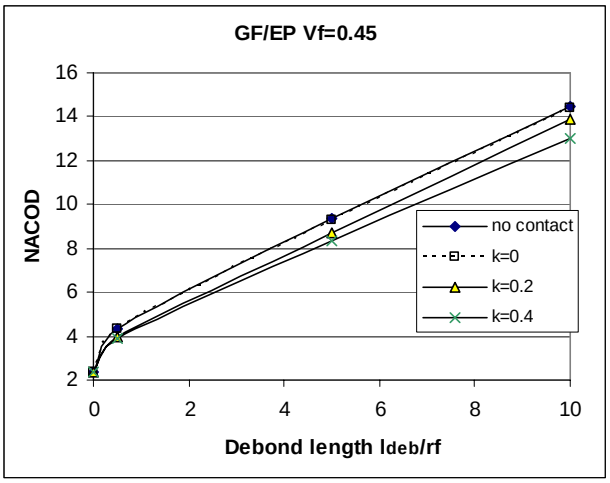

Figure 2.10 *Normalized average COD dependence on the normalized debond length* l_{deb}/r_f *in glass fiber/ epoxy composite. Solution without contact elements and solutions with contact elements and three values of frictional coefficient* k.

Comparing the u_{1an} values of the linear fit at $l_{deb}/r_f = 0$ with the value u_{1an}^b for the bonded case, $l_{deb} = 0$ considered earlier we see that the ratio is almost the same for carbon fiber and glass fiber case (1.51 and 1.47 respectively). Based on this observation we roughly assume that this ratio is material independent and equal to 1.5 and D can be written as

$$D = 1.5u_{1an}^b \tag{2.39}$$

Substitution in (2.38) leads to

$$u_{1an} = 1.5u_{1an}^b + \frac{l_d}{r_f} \tag{2.40}$$

The validity of this expression for fiber contents different than 0.45 has been proved using FEM. The predictions and values from FEM for friction coefficient $k = 0.2$ are presented in Fig. 2.11 and they are in a very good agreement. Eq (2.40) will be used in the following section to predict stiffness reduction in UD composite.

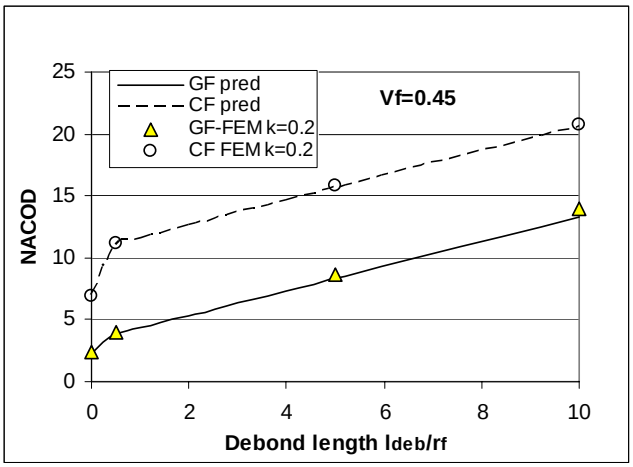

Figure 2.11 *Normalized average COD of fiber cracks with debonds. Predicted (2.40) (lines) and FEM with contact elements and friction coefficient* $k = 0.2$ *(symbols).*

Detailed FEM analysis of fiber crack displacements with debonds $0 < l_{deb} < 0.5 r_f$ was not performed. The following fitting expression may be obtained in this region if we assume linear COD dependence on the debond length

$$u_{1an} = u_{1an}^{b} + \left(u_{1an}^{b} + 1\right)\frac{l_d}{r_f} \tag{2.41}$$

2.6. Stiffness reduction due to fiber breaks in a unidirectional layer.

The fiber crack face sliding displacements as well as the normal displacements of the debond cracks were not investigated in this study. However, as checked by putting arbitrary values in the model, they mainly affect the transverse and shear properties of the UD composite and their effect on the composite longitudinal modulus, is negligible.

The main focus in this paper is the combined effect of fiber breaks and the accompanied debonding on the longitudinal modulus of the composite. This property is affected by the resultant fiber crack opening displacement, COD, only. On the other hand from the

performed calculations using the developed model follows that COD has a negligible effect on other stiffness properties than the longitudinal modulus.

Stiffness reduction predictions were performed for carbon fiber composite with fiber properties $E_{fL} = 300GPa$, $E_{fT} = 30GPa$, $G_{fLT} = 20GPa$, $\nu_{fLT} = 0.2$ and for glass fiber composite with fiber properties $E_f = 70GPa, \nu_f = 0.2$. Matrix was the same for both composites with $E_m = 3GPa$, $\nu_m = 0.4$. Fiber content in the composites was $V_f = 0.5$ and fiber radius $r_f = 4\mu m$.

The statistical fiber cracking evolution with load was not simulated and neither the debond crack growth with load or number of cycles. This type of analysis would give the stiffness changes as a function of the load history.

In this paper the main emphasis is on understanding of the significance of fiber breaks. Hence the damage state in following predictions is used as an input parameter. The number of cracks in all fibers of the RVE can be assumed the same. Predictions are presented in Fig. 2.12 as the normalized longitudinal modulus reduction versus the fiber break density in one fiber measured as the number of fiber breaks per 1cm. The representation of the damage state by crack density does not limit the accuracy because the cracks are considered noninteractive and hence the COD does not depend on the particular location of the fiber crack. Therefore the result is the same for evenly spaced cracks and for arbitrary distributed. The highest number of breaks (20cr/cm correspond to fiber fragment length 0f 0.5mm where the stress perturbations from both ends of the fiber fragment start to interact and the used expressions for COD's are overestimated. The results obtained for three values of the normalized debond length l_{deb} / r_f show that the debond length has a great significance for the stiffness reduction. The relative modulus reduction in carbon fiber composites is larger due to a larger opening of the fiber crack which is a consequence of higher fiber and matrix modulus ratio leading also to larger extent of the stress transfer zone.

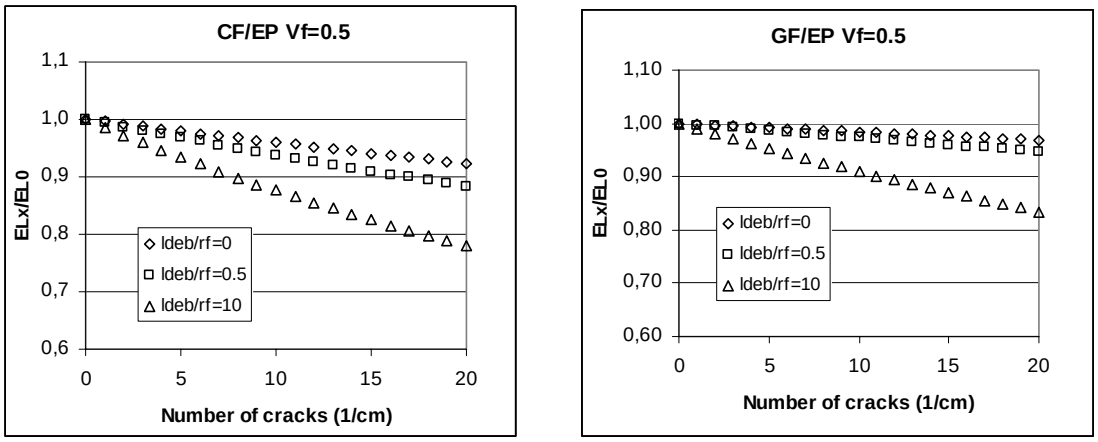

a) b)

Figure 2.12. *Longitudinal modulus reduction in UD composite in a normalized form as a function of the number of fiber breaks in one fiber: a) CF/EP composite, b) GF/EP composite*

2.7 Conclusions for Chapter 2

Stiffness reduction in unidirectional composites due to fiber breaks with a partial interface debonding can be analyzed by the presented model which is based on exact expressions relating the composite stiffness with the normalized average displacements of the fiber crack faces.

Only the opening displacements were studied leaving the sliding effect to further studies. It was found by using arbitrary values that fiber crack face sliding does not affect the longitudinal modulus of the composite. The axial sliding of the debond crack faces is already included through the increased opening of the fiber crack. On the other hand the crack opening does not affect the Poisson's ratio, transverse modulus and shear modulus of the composite.

The main parameters affecting the normalized fiber crack opening have been analyzed using FEM and it is found that the fiber longitudinal modulus, fiber content and the debond length are of the highest significance. These relationships are described by simple functions which excellently fit the numerical results. The effect of other less important parameters is also included in these fitting expressions.

It was found that the relative longitudinal modulus reduction in carbon fiber composite is slightly higher than in glass fiber composite. This trend holds for all considered debond lengths and is related to higher longitudinal modulus/matrix modulus ratio for carbon fibers leading to larger crack openings and larger stress perturbation zones.

Appendix 1

Average stresses and strains over the domain with volume V are defined as follows

$$\{\sigma\}^a = \frac{1}{V}\int_V \{\sigma\} dV \tag{A1.1}$$

$$\{\varepsilon\}^a = \frac{1}{V}\int_V \{\varepsilon\} dV \tag{A1.2}$$

Superscript a denotes the volume average.

Boundary average stress, which has the meaning of the macroscopic stress applied to the external surface S_E of a domain with volume V (in present study it is the average stress applied to the RVE of the UD composite, $V = V_{RVE}$, $S_E = S_{E(RVE)}$, is defined as

$$\sigma_{ij}^{RVE} = \frac{1}{V_{RVE}} \int_{S_{E(RVE)}} \sigma_{ik} n_k x_j dS \tag{A1.3}$$

It is easy to prove (Allen et al., 1998) that the boundary averaged stress is equal to the boundary averaged stress. Hence

$$\{\sigma\}^{RVE} = \{\sigma\}^a \tag{A1.4}$$

Since volume integral over volume V can be written as a sum of integrals over subdomains of this volume (elements) with volume V_k^{el}, one can write

$$\{\sigma\}^a = \sum_k V_k \{\sigma\}_a^k \tag{A1.5}$$

In (A1.5) V_k is the volume fraction of the k-th sub domain.

Boundary averaged strains may be introduced as

$$\varepsilon_{uj}^{ba} = \frac{1}{V}\int_S \frac{1}{2}\left(u_i n_j + u_j n_i\right) dS \tag{A1.6}$$

Also the volume averaged strains are equal to boundary averaged strains (Allen et al., 1998). Since the boundary includes also crack surface ($S = S_E + S_C$) this equality may be written in the following vectorial form

$$\{\varepsilon\}^a = \{\varepsilon\}^{ba} + \{\beta\} \quad \text{or} \quad \begin{Bmatrix} \varepsilon_1 \\ \varepsilon_2 \\ \gamma_{12} \end{Bmatrix}^a = \begin{Bmatrix} \varepsilon_1 \\ \varepsilon_2 \\ \gamma_{12} \end{Bmatrix}^{ba} + \begin{Bmatrix} \beta_{11} \\ \beta_{22} \\ 2\beta_{12} \end{Bmatrix} \tag{A1.7}$$

Here the upper index "ba" stays for "boundary average" over the external boundary. It describes the apparent strain due to the deformation of the outer boundaries. For RVE it is the applied strain. For sub-domains of the RVE (elements) its determinations is in general a complex problem. For elements like layers in laminates, where iso-strain hypothesis is valid this strain is equal to the strain applied to the laminate.

In (A7) β_{ij} is the Vakulenko-Kachanov tensor defined by

$$\beta_{ij} = \frac{1}{V}\int_{S_C} \frac{1}{2}\left(u_i n_j + u_j n_i\right) dS \tag{A1.8}$$

S_c is the total surface of cracks in the domain under consideration, u_i are displacements of the points on the crack surface, n_i is outer normal to the crack surface, In domain with no cracks, β_{ij} is zero.

The stress-strain relationship of the k-th element (2.1) can be averaged over this element, leading to

$$\{\sigma\}_k^a = [Q]_k \{\varepsilon\}_k^a \tag{A1.9}$$

Appendix 2

The $[H]_k$ -matrix is defined in the local axes of an element (fiber and matrix cylinders) and it defines the relationship between k-th element boundary averaged strains and the strains applied to the RVE.

$$\{\varepsilon\}_k^{ba} = [H]_k \{\varepsilon\}_{RVE} \tag{A2.1}$$

The following consideration is for non-damaged elements.

Since in UD composite each element has a form of a cylinder (with an axis in the L-direction) extending in this direction over the whole length of the RVE, some conclusions regarding the form of the $[H]_k$ -matrix can be formulated considering elementary loading cases.

1. $\varepsilon_L^{RVE} \neq 0$, the rest of RVE strains is zero.

Since the strain in each element in the L-direction is equal to the applied strain, the elements $H_{11}^f = H_{11}^m = 1$.

2. Applying ε_T^{LAM} only (with zero RVE longitudinal and shear strain).

The average strain in the L-direction in the element is equal to this strain component applied to the RVE (it is zero). Hence $H_{12}^f = H_{12}^m = 0$.

3. We assume that only applied RVE shear strains may cause non-zero boundary averaged shear strains in the element leading to $H_{16} = H_{26} = H_{61} = H_{62} = 0$.

The rest of elements in the H-matrix depend on geometrical and stiffness parameters and come from solution of a complex 3-D problem. Hence the form of the H-matrix for fiber and for matrix is a s follows

$$[H]_f = \begin{bmatrix} 1 & 0 & 0 \\ H_{21}^f & H_{22}^f & 0 \\ 0 & 0 & H_{66}^f \end{bmatrix} \qquad [H]_m = \begin{bmatrix} 1 & 0 & 0 \\ H_{21}^m & H_{22}^m & 0 \\ 0 & 0 & H_{66}^m \end{bmatrix} \tag{A2.2}$$

H-matrix elements in the fiber and in the resin are not independent.

One relationship between them may be obtained using the request of thermodynamics that the RVE stiffness matrix of the undamaged UD composite, see (2.13) has to be symmetric. For a UD composite the following matrix has to be symmetric

$$V_f\begin{bmatrix} Q_{11}^f & Q_{12}^f & 0 \\ Q_{12}^f & Q_{22}^f & 0 \\ 0 & 0 & Q_{66}^f \end{bmatrix}\begin{bmatrix} 1 & 0 & 0 \\ H_{21}^f & H_{22}^f & 0 \\ 0 & 0 & H_{66}^f \end{bmatrix}+V_m\begin{bmatrix} Q_{11}^m & Q_{12}^m & 0 \\ Q_{12}^m & Q_{22}^m & 0 \\ 0 & 0 & Q_{66}^m \end{bmatrix}\begin{bmatrix} 1 & 0 & 0 \\ H_{21}^m & H_{22}^m & 0 \\ 0 & 0 & H_{66}^m \end{bmatrix} \tag{A2.3}$$

Performing matrix multiplication leads to expression

$$V_f\begin{bmatrix} Q_{11}^f + H_{21}^f Q_{12}^f & Q_{12}^f H_{22}^f & 0 \\ Q_{12}^f + H_{21}^f Q_{22}^f & Q_{22}^f H_{22}^f & 0 \\ 0 & 0 & Q_{66}^f H_{66}^f \end{bmatrix}+V_m\begin{bmatrix} Q_{11}^m + H_{21}^m Q_{12}^m & Q_{12}^m H_{22}^m & 0 \\ Q_{12}^m + H_{21}^m Q_{22}^m & Q_{22}^m H_{22}^m & 0 \\ 0 & 0 & Q_{66}^m H_{66}^m \end{bmatrix} \tag{A2.4}$$

The symmetry means that

$$V_f\left(Q_{12}^f + H_{21}^f Q_{22}^f\right)+V_m\left(Q_{12}^m + H_{21}^m Q_{22}^m\right)=V_f Q_{12}^f H_{22}^f + V_m Q_{12}^m H_{22}^m \tag{A2.5}$$

According to Appendix 1 the strains applied to RVE of an undamaged composite are equal to the volume averaged strains in the RVE which can by expressed by rule of mixture through volume average strains in sub-domains (fiber and matrix). Since the volume averaged strain of the sub-domain equals to its boundary averaged strain we obtain

$$\begin{Bmatrix} \varepsilon_L^0 \\ \varepsilon_T^0 \\ \gamma_{LT}^0 \end{Bmatrix}_{RVE} = V_f\begin{Bmatrix} \varepsilon_L \\ \varepsilon_T \\ \gamma_{LT} \end{Bmatrix}_f^{ba} + V_m\begin{Bmatrix} \varepsilon_L \\ \varepsilon_T \\ \gamma_{LT} \end{Bmatrix}_m^{ba} \tag{A2.6}$$

Expressing boundary averaged strains in (A2.6) through RVE strain using (2.6) leads to

$$\begin{Bmatrix} \varepsilon_L^0 \\ \varepsilon_T^0 \\ \gamma_{LT}^0 \end{Bmatrix}_{RVE} = \left(V_f\begin{bmatrix} 1 & 0 & 0 \\ H_{21}^f & H_{22}^f & 0 \\ 0 & 0 & H_{66}^f \end{bmatrix}+V_m\begin{bmatrix} 1 & 0 & 0 \\ H_{21}^m & H_{22}^m & 0 \\ 0 & 0 & H_{66}^m \end{bmatrix}\right)\begin{Bmatrix} \varepsilon_L^0 \\ \varepsilon_T^0 \\ \gamma_{LT}^0 \end{Bmatrix}_{RVE} \tag{A2.7}$$

The longitudinal strain relationship in (A2.7) is satisfied automatically. The transverse strain relationship (second equation in (A2.7)) leads to

$$\varepsilon^0_{T,RVE} = V_f\left(H^f_{21}\varepsilon^0_{L,RVE} + H^f_{22}\varepsilon^0_{T,RVE}\right) + V_m\left(H^m_{21}\varepsilon^0_{L,RVE} + H^m_{22}\varepsilon^0_{T,RVE}\right) \tag{A2.8}$$

Comparing coefficients in terms related with $\varepsilon^0_{L,RVE}$ and $\varepsilon^0_{T,RVE}$ respectively we obtain to relationships

$$V_f H^f_{21} + V_m H^m_{21} = 0 \qquad V_f H^f_{22} + V_m H^m_{22} = 1 \tag{A2.9}$$

From (A2.9) follows relationships between H-matrix elements in the fiber and matrix

$$H^m_{21} = -H^f_{21}\frac{V_f}{V_m} \qquad H^m_{22} = \frac{1 - V_f H^f_{22}}{V_m} \tag{A2.10}$$

Substituting (A2.10) in (A2.5) we obtain

$$H^f_{21} = \left(H^f_{22} - 1\right)\frac{Q^f_{12} - Q^m_{12}}{Q^f_{22} - Q^m_{22}} \tag{A2.11}$$

Considering the shear strain relationship in (A2.7) we obtain

$$H^m_{66} = \frac{1 - V_f H^f_{66}}{V_m} \tag{A2.12}$$

Estimations may be obtained using Concentric Cylinder Assembly model by Hashin et al., (1964), Hashin, (1983) or numerical solutions

REFERENCES

Abdelrahman, W.G. and Nayfeh, A.H. 1999. "Stress transfer and stiffness reduction in orthogonally cracked laminates", *Mech. Mater*., 31:303-316.

Allen, D.H., Harris, C.E. and Groves, S.E. 1987. "A thermomechanical constitutive theory for elastic composites with distributed damage. Part II: application to matrix cracking in laminated composites", *Int. J. Solids Struct*., 23:1319-1338.

Allen, D.H. and Yoon, C. 1998. "Homogenization techniques for thermo-viscoelastic solids containing cracks", *Int. J. Solids Struct*., 35:4035-4053.

Cox, H.L.,1952, "The elasticity and strength of paper and other fibrious materials", Brit. J. Appl. Phys., 3, 72-79.

Dvorak GJ, Laws N, Hejazi M., 1985, Analysis of progressive matrix cracking in composite laminates I. Thermoelastic properties of a ply with cracks, J Comp Mater, 19: 216-234.

Gudmundson, P. and Östlund, S. 1992. "First order analysis of stiffness reduction due to matrix cracking", *J. Comp. Mater.,* 26:1009-1030.

Gudmundson, P. and Zang, W. 1993. "A universal model for thermoelastic properties of macro cracked composite laminates", *Int. J. Solids Struct*., 30:3211-3231.

Hashin Z, Rosen BW., 1964, "The elastic moduli of fiber-reinforced materials", Journal of Applied Mechanics, 31(2), 223-232.

Hashin Z., 1983, "Analysis of Composite Materials – a Survey", Journal of Applied Mechanics, 50, 481-505.

Hashin, Z. 1985. "Analysis of cracked laminates: a variational approach", *Mech. Mater*., North-Holland 4:121-136.

Hashin, Z. 1987. "Analysis of Orthogonally Cracked Laminates Under Tension", *J. Appl. Mech*., 54:872-879.

Henaff-Gardin, C., Lafarie-Frenot, M.C. and Gamby, D. 1996. "Doubly periodic matrix cracking in composite laminates Part 1: General in-plane loading". *Comp. Struct*., 36:113-130.

Herakovich CT, Aboudi J, Lee SW, Strauss EA. Damage in composite laminates: effects of transverse cracks, Mech of Mater, 1988; 7: 91-107.

Horii H, Nemat-Nasser S., 1980, Overall moduli of solids with microcracks: Load induced anisotropy. J Mech Phys Solids, 31:155-177.

Hua Yu, Wang Xingguo, Li Zhengneng, He Qingzhi, Property degradation of anisotropic composite laminates with matrix cracking. Part I: Development of constitutive relations for $(\theta_m/90_n)$s cracked laminates by stiffness partition, J Reinf Plast and Comp, 1996;15:1146-1160.

Jinghong Fan, Junqian Zhang, 1993, In-situ damage evolution and micro/macro transition for laminated composites, Comp Sci Technol, 47:107-118.

Joffe, R., Krasnikovs, A. and Varna, J. 2001. "COD-based simulation of transverse cracking and stiffness reduction in [S/90n]s laminates", *Comp. Sci. Tech.,* 61:637-656.

Kashtalyan M, Soutis C., 2000, Stiffness degradation in cross-ply laminates damaged by transverse cracking and splitting, Composites Part A: 31:335-351.

Kashtalyan M, Soutis C., 2002, Mechanisms of internal damage and their effect on the behavior and properties of cross-ply composite laminates, Int Appl Mech, 38(6): 641-657.

Kim, R.Y., Crasto, A.S. and Schoeppner, G.A. 2000. "Dimensional stability of composite in space thermal environment", *Comp. Sci. Tech*., 60:2601-2608.

Ladeveze, P.1990. "A damage mechanics for composite materials", In: Integration of theory and application in applied mechanics. Dordrecht: Kluver, 13-24.

Lundmark P, Varna J. 2003, Modeling thermo-mechanical properties of damaged laminates. *Key Eng Mater*, 251-252:381-387.

Lundmark P, Varna, J. 2005, Constitutive relationships for damaged laminate in in-plane loading. *Int J Dam Mech*, 14(3):235-259.

Lundmark P. and J. Varna, 2006, "Crack face sliding effect on stiffness of laminates with ply cracks", Composites Science and Technology, 66, 1444-1454

McCartney L.N., 1987, "Mechanics of matrix cracking in brittle matrix fiber reinforced composites", Proc. R. Soc. Lond,. A409, 329-350

McCartney, L.N. 1992. "Theory of stress transfer in 0-90-0 crossply laminate containing a parallel array of transverse cracks", *J. Mech. Phys. Solids*, 40:27-68.

McCartney, L.N. 1995. "A recursive method of calculating stress transfer in multiple-ply cross-ply laminates subject to biaxial loading", NPL report DMMA(A)150.

McCartney, L.N. and Schoeppner, G.A. and Becker, W. 2000. "Comparison of models for transverse ply cracks in composite laminates", *Comp. Sci. Tech*., 60:2347-2359.

Nairn, J.and Hu, S. 1994. “Matrix microcracking . In: Pipes R.B, Talreja R, editors. *Comp. Mater*. series, vol. 9. *Dam. Mech. Comp. Mater*. Amsterdam: Elsevier, 187-243.

Nairn, J. 2000. “Matrix microcracking in composites”, In: Kelly A, Zweben C, Talreja R, Manson J-A, editors. *Compr. Comp. Mater*., vol. 2. *Poly. Matrix Comp*., Amsterdam: Elsevier, 403-432.

Nuismer RJ, Tan SC. Constitutive relations of a cracked composite lamina. J Comp Mater, 1988;22:306-321.

Schoeppner, G.A and Pagano, N. 1998. “Stress fields and energy release rates in cross-ply laminates”, *Int. J. Solids Struct*., 35(11):1025-1055.

Tan SC, Nuismer RJ. A theory for progressive matrix cracking in composite laminates, J Comp Mater, 1989;23:1029-1047.

Tao JX, Sun CT., 1996, Effect of matrix cracking on stiffness of composite laminates. Mech Comp Mater and Struct. 1996;3:225-239.

Talreja, R. 1994. “Damage characterization by internal variables”. In: Pipes R.B, Talreja R, editors. *Comp. Mater*. series, vol. 9. *Dam. Mech. Comp. Mater.,* Amsterdam: Elsevier, 53-78.

Talreja, R.1996. “A synergistic damage mechanics approach to durability of composite material systems”, In: Cardon A, Fukuda H, Reifsnider K, editors. Progress in durability analysis of composite systems. Rotterdam: A.A. Balkema, 117- 129.

Tsai CL, Daniel IM. The behaviour of cracked cross-ply composite laminates under shear loading. Int J Sol Struct. 1992;29(24):3251-3267.

Tsai CL, Daniel IM, Lee JW, 1990, Progressive matrix cracking of crossply composite laminates under biaxial loading. In: Microcracking-Induced Damage in Composites, Ed G.J. Dvorak and D.C. Lagoudas. Proc. Of ASME: 1990 Winter Annual Meeting. AMD-vol.111, MD-vol. 22. pp.9-18. ASME, New York.

Varna, J., Berglund, L.A., Talreja, R. and Jakovics, A. 1993. “A study of the crack opening displacement of transverse cracks in cross-ply laminates”, *Int. J. Dam. Mech*., 2:272-289.

Varna, J., Akshantala, N.V. and Talreja, R. 1999. “Crack opening displacement and the associated response of laminates with varying constraints”, *Int. J. Dam. Mech*., 8:174-193.

Varna, J., Joffe, R., Akshantala, N.V. and Talreja, R. 1999. “Damage in composite laminates with off-axis plies”, *Comp. Sci. Tech*., 59:2139-2147.

Varna, J., Joffe, R. and Talreja, R. 2001. "A synergistic damage mechanics analysis of transverse cracking in [±θ,904]s laminates", *Comp. Sci. Tech*., 61:657-665.

Varna, J. 2002. "Effective properties of damaged laminated composites reinforced with continues UD fibers", Proceedings of the 10th European Conference on Composite Materials, Brugge, Belgium, paper 270.

Varna, J., Krasnikovs, A., Kumar, R. and Talreja R. 2003. "A Synergistic damage mechanics approach to viscoelastic response of cracked cross-ply laminates", *Int. J. Dam. Mech,*, International Journal of Damage Mechanics, (2004);13: 301-334.

Wu, W., Verpoest, I. & Varna, J., 1998, "A novel axisymmetric variational analysis of the stress transfer into fibre through a partially debonded interface", Composites Science and Technology, 58, 1863-1877.

Xia Z.X., Curtin W.A., 2002, "Shear-lag vs. Finite element models for stress transfer in fiber-reinforced composites", Composites Science and Technology, 62, 1141-1149.

Zhang J, Fan J, Soutis C. Analysis of multiple matrix cracking in $[\pm\theta_m/90_n]$s composite laminates. Part 1. In-plane stiffness properties, Composites, 1992;23(5): 291-304.